



HAL
open science

FGF10 promotes cardiac repair through a dual cellular mechanism increasing cardiomyocyte renewal and inhibiting fibrosis

Fabien Hubert, Sandy Payan, Edeline Pelce, Laetitia Bouchard, Rachel Sturny, Nicolas Lenfant, Giovanna Mottola, Frédéric Collart, Robert Kelly, Francesca Rochais

► To cite this version:

Fabien Hubert, Sandy Payan, Edeline Pelce, Laetitia Bouchard, Rachel Sturny, et al.. FGF10 promotes cardiac repair through a dual cellular mechanism increasing cardiomyocyte renewal and inhibiting fibrosis. *Cardiovascular Research*, 2022, 118 (12), pp.2625-2637. 10.1093/cvr/cvab340 . hal-03654648

HAL Id: hal-03654648

<https://amu.hal.science/hal-03654648>

Submitted on 8 Feb 2023

HAL is a multi-disciplinary open access archive for the deposit and dissemination of scientific research documents, whether they are published or not. The documents may come from teaching and research institutions in France or abroad, or from public or private research centers.

L'archive ouverte pluridisciplinaire **HAL**, est destinée au dépôt et à la diffusion de documents scientifiques de niveau recherche, publiés ou non, émanant des établissements d'enseignement et de recherche français ou étrangers, des laboratoires publics ou privés.

1 **FGF10 promotes cardiac repair through a dual cellular mechanism**
2 **increasing cardiomyocyte renewal and inhibiting fibrosis**

3
4 Fabien Hubert PhD ^{1#}, Sandy M Payan PhD ^{1#}, Edeline Pelce MD-MSc ^{1,2}, Laetitia Bouchard
5 MSc ¹, Rachel Sturny ³, Nicolas Lenfant PhD ¹, Giovanna Mottola PhD ^{4,5}, Frédéric Collart
6 MD ², Robert G Kelly PhD ³ and Francesca Rochais PhD ¹

7
8 ¹ Aix Marseille Univ, INSERM, MMG, U 1251, Marseille, France.

9 ² Department of Cardiac Surgery, Timone Hospital, AP-HM, Marseille, France.

10 ³ Aix Marseille Univ, CNRS UMR 7288, IBDM, Marseille, France.

11 ⁴ Aix-Marseille Univ, C2VN, INSERM 1263, INRAE 1260, Marseille, France.

12 ⁵ Laboratory of Biochemistry, Timone Hospital, Marseille, France.

13 # These authors contributed equally

14
15 **Address for correspondence**

16 Dr. Francesca Rochais, Aix Marseille Université, MMG U1251

17 27 Boulevard Jean Moulin, 13005 Marseille, France

18 Phone : +334 91 32 48 86 ; FAX : +334 91 79 72 27

19 francesca.rochais@univ-amu.fr

20

21 Short Title: FGF10 promotes cardiac repair and regeneration

22 Original Article

23 Total word count: 8397

24 **ABSTRACT**

25

26 **Aims.** Promoting cardiomyocyte renewal represents a major therapeutic approach for heart
27 regeneration and repair. Our study aims to investigate the relevance of FGF10 as a potential
28 target for heart regeneration.

29 **Methods and Results.** Our results first reveal that *Fgf10* levels are upregulated in the injured
30 ventricle after MI. Adult mice with reduced *Fgf10* expression subjected to MI display impaired
31 cardiomyocyte proliferation and enhanced cardiac fibrosis, leading to a worsened cardiac
32 function and remodeling post-MI. In contrast, conditional *Fgf10* overexpression post-MI
33 revealed that, by enhancing cardiomyocyte proliferation and preventing scar-promoting
34 myofibroblast activation, FGF10 preserves cardiac remodeling and function. Moreover, FGF10
35 activates major regenerative pathways including the regulation of *Meis1* expression levels, the
36 Hippo signaling pathway and a pro-glycolytic metabolic switch. Finally, we demonstrate that
37 elevated *FGF10* levels in failing human hearts correlate with reduced fibrosis and enhanced
38 cardiomyocyte proliferation.

39 **Conclusions.** Altogether, our study shows that FGF10 promotes cardiac regeneration and
40 repair through two cellular mechanisms: elevating cardiomyocyte renewal and limiting
41 fibrosis. This study thus identifies FGF10 as a clinically relevant target for heart regeneration
42 and repair in man.

43

44

45

46

47

48 **1. INTRODUCTION**

49

50 Ischemic heart disease is the leading cause of cardiovascular disease death worldwide
51 (1). Myocardial infarction is characterized by dramatic cardiomyocyte loss associated
52 with profound fibrotic scarring and leads to severe impairment of cardiac function and
53 ultimately to congestive heart failure. The existence, in the adult mammalian heart, of low but
54 detectable cardiomyocyte proliferative capacities (2) has oriented regenerative medicine
55 toward new therapeutical strategies. Indeed, the stimulation of terminally differentiated
56 cardiomyocyte proliferation currently represents the main therapeutic approach for heart
57 regeneration (3). Increasing evidence demonstrating that the loss of mammalian
58 cardiomyocyte renewal potential shortly after birth causes the loss of regenerative
59 capacities, strongly support the hypothesis that a detailed understanding of the
60 regulation of fetal cardiomyocyte proliferation is essential to identify targets for
61 cardiac regeneration (4, 5). Cardiac regeneration is a complex process in which, in
62 addition to promoting cardiomyocyte proliferation, preventing mature scar formation is
63 essential. Interestingly, recent evidence investigating endogenous regenerative capacities in
64 lower vertebrates suggests that reducing the fibroblast to myofibroblast transition may
65 result in a softer scar tissue, more compliant to cardiomyocyte renewal and favorable to
66 regeneration (6).

67 We recently uncovered a role for Fibroblast Growth Factor FGF10 signaling in regulating
68 fetal cardiomyocyte proliferation (7). FGF10 is a paracrine FGF family member and is known
69 to play essential roles in the development of multiple organs (8). *Fgf10* is expressed in
70 second heart field (SHF) cardiac progenitor cells in the early embryo, however it is not
71 essential for SHF deployment and subsequent heart tube elongation (9). In contrast, in the
fetal heart, FGF10 controls regionalized cardiomyocyte proliferation through a cell₃
type autonomous

72 mechanism involving FOXO3 transcription factor phosphorylation and subsequent
73 downregulation of the cyclin dependent kinase inhibitor p27^{kip1} expression. As a result, *Fgf10*-
74 null embryos, which die at birth due to lung aplasia, display altered heart morphology (7, 10).
75 Interestingly, forced *Fgf10* expression in adult mice specifically promotes cardiomyocyte cell
76 cycle reentry (7) suggesting that FGF10 may be a potential target to improve the limited innate
77 regenerative capacities of the myocardium after injury. In this study, using an experimental
78 mouse model of myocardial infarction (MI) together with *Fgf10*-gain and loss of function
79 mouse models, we demonstrate that upregulation of *Fgf10* promotes cardiac regeneration
80 and repair post-MI. Our results reveal that this effect is mediated through the elevation of
81 cardiomyocyte proliferation and reduction of fibrosis. Moreover, analysis of *FGF10* expression
82 in failing explanted human hearts revealed a strong correlation between elevated *FGF10*
83 levels, reduced fibrosis and enhanced cardiomyocyte proliferation. Together these
84 experiments identify FGF10 as a potential clinical target to enhance cardiac repair and
85 regeneration.

86
87
88
89
90
91
92
93
94
95
96
97

98 2. METHODS

99

100 2.1 Mice

101 Animal studies were performed according to the guidelines from Directive 2010/63/EU of the
102 European Parliament on the protection of animals used for scientific purposes. Mouse care
103 and procedures were approved by the Departmental Direction of Veterinary Services of the
104 French Ministry of Agriculture and the local ethics committee (APAFIS#84 74-20170 II
105 009244646 v2). *Fgf10^{+/-}*, *Fgf10-LacZ*, *Rosa-tdT*, *α MHC-MerCreMer*, *Rosa26-rtTA* and *Tet(O)-*
106 *Fgf10* mice were maintained on mixed genetic backgrounds. Inducible expression of *Fgf10* is
107 achieved by feeding sequentially mice with food containing doxycycline (625 mg/kg DOX,
108 Envigo). Floxed allele recombination in adult mice was achieved by intraperitoneal tamoxifen
109 injection at a dose per day of 2 mg/30 g for 3 days. The Phire Animal Tissue Direct PCR Kit (Life
110 Technologies) was used to genotype transgenic mice without prior DNA Purification. Extended
111 genotyping procedure can be found in the [Supplemental Data](#). For cardiac tissue collection,
112 mice were euthanized by cervical dislocation.

113

114 2.2 Human heart samples

115 Human tissue samples were provided by the Cardio-Thoracic Surgery Department of La
116 Timone Hospital Marseille, in accordance with the principles outlined in the Declaration of
117 Helsinki and with human research protocol approved by the institution under which patient
118 informed consent was obtained. Human heart tissues were obtained from failing explanted
119 hearts. Patient clinical features are provided in [Supplemental Table 2](#). All patients displayed
120 initial myocardial infarction. Samples were collected in the right ventricle, the infarcted area,
121 border zone and remote area of the freshly explanted heart and immediately processed. All

122 included hearts were arising from patients displaying left ventricular ischemic cardiomyopathy
123 with non-altered right ventricular function.

124

125 **2.3 Myocardial infarction model**

126 Adult mice (3 month-old) were sedated with a mixture of ketamine (100 mg/kg) and xylazine
127 (10 mg/Kg) via intraperitoneal injection, and following endotracheal intubation, were
128 artificially ventilated. If necessary 1-2% isoflurane was added as maintenance anesthetic. For
129 analgesia, buprenorphine. (0.1 mg/kg) was injected subcutaneously 30 min prior surgery.
130 Following skin incision, lateral thoracotomy at the fourth intercostal space was performed by
131 blunt dissection of the intercostal muscles. Under stereomicroscope control, the left anterior
132 descending coronary artery was visualized and ligated (with 8.0 non-absorbable silk suture)
133 2.0 mm below the left atrium, just above the bifurcation of the left diagonal arteries. Effective
134 ligation of the coronary artery was confirmed by whitening of the LV affected region below
135 the ligation site. Out of 145 MI-mice, 30 were excluded due to malpositioning of the ligation.
136 The thoracic wall and skin incisions were then sutured with 6.0 non-absorbable and 4.0
137 absorbable silk sutures, respectively. Mice were then warmed for several minutes until
138 recovery.

139

140 **2.4 Echocardiography**

141 Heart function was evaluated at the CERIMED-Marseille, by transthoracic echocardiography
142 performed on isoflurane-sedated mice using a Vevo 2100 VisualSonics. Mice were anesthetized
143 with isoflurane in oxygen (2% for induction and 1% for maintenance) and placed on a warm pad
144 at the supine position. All echocardiography measurements were performed in a blinded
145 manner.

146 **2.5 Tissue processing**

147 Mouse hearts were dissected and analyzed using a Zeiss Lumar stereo dissecting microscope.
148 For X-gal staining, hearts were collected and fixed for 3 hours in 4% paraformaldehyde
149 (PFA), extensively washed in 1X PBS and stained for 12 hours at 37°C in a solution containing
150 4mg/ml of X-gal. After staining, the samples were washed in PBS, post-fixed in PFA 4% and
151 observed under a Zeiss Lumar stereomicroscope. For immunostaining and sirius red
152 staining, samples were fixed in 4% PFA for 3 hours and extensively washed in 1X PBS.
153 Paraffin embedding was performed following dehydration using a graded ethanol series
154 (50, 70, 90 and 100%), two xylene washes and three paraffin washes (Paraplast X-tra,
155 Sigma P3808). Cryopreservation was achieved by incubation of samples in a sucrose series
156 (15 and 30%) and embedding in OCT (VWR, 361603E). Infarct size was estimated using
157 ImageJ software on 6 sirius red stained sections containing the papillary muscle region and
158 based on the ratio of the length of the left ventricular infarct area showing fibrosis by the
159 total left ventricular length as described before (11). Extended immunostaining and sirius red
160 staining procedures, including antibody list, can be found in the [Supplemental Data](#).
161 Cardiomyocyte proliferation analysis was examined using Ki67, PH3 and AURKB
162 immunofluorescence. The number of Ki67-, PH3- and AURKB-positive nuclei was counted
163 from 8-10 sections per individual heart. Measurements are the average of 5-7 independent
164 hearts for each indicated genotype and treatment.

165

166 **2.6 Quantitative Real Time PCR**

167 Total RNA was extracted using Trizol LS reagent (Life technologies). First strand cDNA was
168 synthesized using Maxima Reverse Transcriptase (Life technologies). qRT-PCR was performed
using the following primers and Luminaris qPCR SuperMix (Life technologies) and a Roche

169 Light Cycler 480. Each experiment was performed in duplicate and normalized to house-
170 keeping gene. Detailed quantitative RT-PCR primers can be found in the [Supplemental Data](#).

171

172 **2.7 Biochemical Analysis of circulating protein levels**

173 DOX-treated *Rosa26-RTTA/Tet(O)-Fgf10* were compared to CTRL-treated *Rosa26-*
174 *RTTA/Tet(O)-Fgf10* infarcted mice, 5 days post-injury. Blood sample was collected into serum
175 separator tube and the serum was coagulated at room temperature for 2 hours. The
176 homogenates were centrifuged at 1000 g for 20 min, and the resultant supernatant was
177 collected and stored at -20°C. Highly sensitive troponin T (TnT-hs, Elecsys®) was measured on
178 COBAS-8000 Roche®, TnT-hs was measured using an immunological sandwich method
179 (detection threshold: 5 pg/ml, range: 5–50 ng, intra-assay variation < 10%; intra-assay range:
180 between 2 and 4%). Circulating FGF10 levels were assessed using Elisa assay according to the
181 manufacturer's protocols (mouse FGF10 ELISA kit, Abxbexa, abx574964), and the absorbance
182 values were detected at 450 nm using a microplate reader. Serum levels of cardiac troponin I
183 were addressed using western blot analysis. Equal amount of protein were subjected to SDS-
184 PAGE. After electrophoresis, proteins were transferred to PVDF membranes and
185 immunoblotted with Troponin I antibody (MAB1691, 1/1000). Proteins were detected by
186 chemiluminescence using a Bio-Rad ChemiDoc analyser. Amido Black staining (Sigma 1.01167)
187 was performed to visualize total protein. Relative densities were quantified using the ImageJ
188 software. All data were normalized by internal controls.

189

190 **2.8 Cardiomyocyte isolation and culture**

191 Ventricular cardiomyocytes were obtained from 10 week-old *aMHC-MerCreMer/R26R-*
192 *Tomato/R26R-RTTA/Tet(O)-Fgf10* males intraperitoneally injected with tamoxifen (2 mg/30 g

193 for 3 days) and the fed with normal (CTRL) or doxycycline (DOX) supplemented food for 5 days.
194 Mice were anesthetized by intraperitoneal injection of a ketamine-xylazine cocktail (ketamine,
195 93.75 mg/kg; xylazine, 12.5 mg/kg), and the chest was opened to expose the heart. The
196 descending aorta and inferior vena cava were cut and the heart was rapidly flushed by
197 injection of EDTA buffer (130 mM NaCl, 5 mM KCl, 0.5 mM NaH₂PO₄, 10 mM HEPES, 10 mM
198 glucose, 10 mM BDM, 10 mM Taurine and 5 mM EDTA adjusted to pH 7.8) in the right
199 ventricle. Ascending aorta was clamped and the heart was immediately transferred to a 60-mm
200 dish containing fresh EDTA buffer. Digestion was achieved by sequential injection of EDTA
201 buffer, perfusion buffer (130 mM NaCl, 5 mM KCl, 0.5 MgCl₂ adjusted to pH 7.8), and finally
202 an enzymatic solution (perfusion buffer supplemented with collagenase 2 and 4 and protease
203 XIV) into the left ventricle. The ventricles were separated from the atria, cut into small pieces,
204 and triturated with a pipette to disperse cardiomyocytes. Ventricular cardiomyocytes were
205 filtered (100 µm pore size filter) and allowed to sediment by gravity for 20 minutes. The
206 supernatant was removed, and cells were suspended in three intermediate calcium
207 reintroduction buffers (0.34, 0.68 and 1.02 mmol/l Ca²⁺) to gradually restore calcium
208 concentration to physiological levels. At the end, ventricular cardiomyocytes were
209 resuspended in a culture medium and plated in culture dishes coated with laminin (Life
210 Technologies, 10 µg/ml).

211

212 **2.9 Cell culture and pharmacological stimulations**

213 Human cardiac fibroblast (HCF) cell line (Promocell®, C-12375) was cultured in Fibroblast
214 Growth Medium 3 (Promocell®, C-23025). Cells were maintained at 37°C in a 95% air-5% CO₂
215 humidified atmosphere, fed every 2–3 days, and sub-cultured when reaching 70–80%. HCF

216 were treated with TGF- β 1 (Miltenyi Biotec, 5 μ g/ml) and recombinant FGF10 (R&D Systems,
217 100ng/ml).

218

219 **2.10 RNA sequencing**

220 Sequencing and bioinformatics analysis were performed by the Genomics and Bioinformatics
221 facility (GBiM) from the U 1251/Marseille Medical Genetics. RNA-Seq was performed in
222 quadruplicate on DOX-treated *Rosa26-RTTA/Tet(O)-Fgf10* infarcted area 21 days post-injury
223 as compared to the same area from CTRL-treated *Rosa26-RTTA/Tet(O)-Fgf10*. Before
224 sequencing, the quality of total RNA samples was assessed using a bioanalyzer (Agilent, Santa
225 Clara, California, USA). Only RNAs with RNA Integrity Numbers (RIN) above 8 were used. For
226 each sample, a library for poly(A)+ RNA was prepared from 1 μ g of total RNA, using the TruSeq
227 Stranded mRNA Library Prep kit (Illumina, San Diego, California, USA), following the
228 manufacturer's instructions. The 8 indexed libraries were pooled and sequenced on an
229 Illumina NextSeq 500 platform, using paired-end mode (2*75 bp reads), in order to reach 50
230 million reads (clusters) for each library. Detailed data processing and differential gene
231 expression (DGE) analysis can be found in the [Supplemental Data](#).

232

233 **2.11 Statistics**

234 All experiments and data analysis were conducted blinded. The number of replicates (n) is
235 indicated in the figure legends and refers to the number of experimental subjects
236 independently treated in each experimental condition. Data are presented as means \pm s.e.m.
237 Statistical significance (p) was determined using unpaired Student's *t*-test, Student's *t*-
238 distribution and Fisher test, as indicated in each figure legend. Statistical significance was set
239 at *p < 0.05, 0.001 < **p < 0.01, ***p < 0.001.

240 3. RESULTS

241

242 3.1 *Fgf10* upregulation following MI

243 To study the role of FGF10 in ischemic heart disease, we first analyzed cardiac *Fgf10*
244 expression in mice subjected to myocardial infarction (MI) through ligation of the left anterior
245 descending coronary artery. 21 days after ligation, mice were sacrificed, hearts were removed
246 and qRT-PCR experiments revealed upregulated endogenous *Fgf10* levels in the injured
247 ventricle (Fold Change (FC)=3.5; [Supplemental Figure 1A](#)). Analysis of cryostat sections from
248 *Fgf10-LacZ* hearts 21 days post-MI showed that X-gal⁺ nuclei are exclusively present in
249 cardiomyocytes (data not shown), suggesting that *Fgf10* expression is upregulated in
250 cardiomyocytes under pathological conditions. Directly controlled by key developmental
251 transcription factors including NKX2-5, TBX1 and ISL1, a cardiac enhancer, located in the first
252 intron of *Fgf10* gene, has been identified and described to be necessary and sufficient to direct
253 *Fgf10* expression in the developing heart. While ISL1 and TBX1 activate *Fgf10* expression in
254 cardiac progenitor cells, NKX2-5 mediates its repression (12). In order to address a potential
255 involvement of NKX2-5, TBX1 and ISL1 in the upregulation of *Fgf10* expression post-MI, we
256 evaluated *Nkx2-5*, *Tbx1* and *Isl1* expression in the injured ventricle. Interestingly, while *Nkx2-*
257 *5* expression levels were downregulated ([Supplemental Figure 1B](#)), strong upregulation of
258 *Tbx1* and *Isl1* mRNA levels was observed 21 days post-MI ([Supplemental Figure 1C-D](#)).
259 Consistent with cardiomyocyte dedifferentiation prior to cell cycle release (13-16), our results
260 thus suggest that reactivation of the transcriptional embryonic program may drive *Fgf10*
261 expression under pathological conditions.

262

263

264 **3.2 Decreased *Fgf10* dosage worsens cardiac function and remodeling following MI**

265 In order to evaluate the role of upregulated *Fgf10* levels under pathological conditions, mice
266 with reduced *Fgf10* expression (FC=0.56; p=0.006; WT, n=5; *Fgf10*^{+/-}, n=5) were subjected to
267 MI (Figure 1A). Compared to WT-MI infarcted area, *Fgf10* expression levels in *Fgf10*^{+/-}-MI
268 infarcted area 21 days post-MI were significantly reduced (FC=0.2; p=0.005; WT-MI, n=5;
269 *Fgf10*^{+/-}-MI, n=6). 21 days after MI, infarct size measurement (*Fgf10*^{+/-}-MI: 30±8% over WT-
270 MI, p=0.02), together with heart/body weight and heart weight/tibia length ratios (Figure 1B-
271 C) revealed significant worsening of cardiac remodeling in *Fgf10*^{+/-}-MI compare to WT-MI
272 mice. *In vivo* heart function was investigated using echocardiography (Figure 1D). Compared
273 to WT infarcted mice, *Fgf10*^{+/-} infarcted mice displayed worsened cardiac performance
274 including a further decreased ejection fraction and fractional shortening and a further
275 increased left ventricular volume (Figure 1E-G). Analysis of key heart failure marker expression
276 using qRT-PCR experiments confirmed the worsened pathological remodeling in *Fgf10*^{+/-}-MI
277 compare to WT-MI mice (Figure 1H). Together, these results reveal that maximal FGF10 levels
278 play a protective role in ischemic heart failure.

279

280 **3.3 Decreased *Fgf10* dosage impairs cardiomyocyte proliferation and worsens fibrosis** 281 **following MI**

282 To determine whether upregulated *Fgf10* levels in the injured ventricle could participate in
283 cardiomyocyte renewal post-MI, cardiac cell proliferation was analyzed, in *Fgf10*^{+/-}-MI
284 compare to WT-MI mice, 5 and 21 days (Figure 2A) post-MI. Immunofluorescence analysis of
285 proliferative capacity in the border zone (BZ), using the pan-cell cycle marker Ki67 (Figure 2B-
286 D and supplemental Figure 2A), the mitotic marker PH3 (Supplemental Figure 2B-D) and the
287 cytokinesis marker Aurora kinase B (AURKB, Figure 2E), revealed a significant impairment of

288 cardiomyocyte proliferation in *Fgf10*^{+/-}-MI compare to WT-MI mice. Similar results were
289 obtained when cardiomyocyte proliferation was measured in the infarcted area (IA;
290 [Supplemental Figure 2E-F](#)). No alteration in non-myocyte proliferation capacity was detected
291 ([Supplemental Figure 2G-H](#)). Measurement of cardiomyocyte cross-sectional area revealed
292 that decreased *Fgf10* dosage significantly worsens cardiomyocyte hypertrophy post-MI
293 ([Figure 2F](#)). To determine whether FGF10 haploinsufficiency impacts on the progression of
294 cardiac fibrosis following MI, histological analysis using Sirius red staining was performed. At
295 both 5 ([Figure 2G-I](#)) and 21 days ([Figure 2J-L](#)) post-MI, increased fibrosis was observed in
296 *Fgf10*^{+/-}-MI hearts compare to WT-MI hearts, correlating with upregulated collagen gene
297 expression ([Figure 2I and L](#)). Together, these results suggest that maximal *Fgf10* levels
298 promote cardiomyocyte renewal and prevent fibrosis post-MI, likely contributing to preserved
299 cardiac function and decreased remodeling.

300

301 **3.4 *Fgf10* upregulation following MI preserves cardiac performance**

302 In order to determine whether forced *Fgf10* expression after MI would promote cardiac
303 regeneration and repair, we took an inducible gain-of-function approach. As FGF10 is a
304 secreted molecule, global and temporal conditional overexpression of *Fgf10* was achieved
305 using the *Rosa26-RTTA/Tet(O)-Fgf10* mouse line treated with doxycycline-supplemented
306 (DOX) food one day after MI during 21 days ([Figure 3A](#)). *Rosa26-RTTA/Tet(O)-Fgf10* DOX-MI
307 mice were compared with *Rosa26-RTTA/Tet(O)-Fgf10* mice treated with control food (CTRL-
308 MI) and qRT-PCR experiments on left ventricular tissues and biochemical analysis of serum
309 post-MI confirmed that DOX-treated mice displayed significantly upregulated myocardial
310 (FC=106, $p=7 \times 10^{-6}$, $n=4$ per group) and circulating *Fgf10* levels (DOX-MI: 3.1 ± 0.2 ng/ml versus
311 CTRL-MI: 1.9 ± 0.2 ng/ml; $p=0.007$, $n=4$ per group). Our results demonstrated that *Fgf10*

312 upregulation prevents cardiac remodeling 21 days after MI, as depicted by infarct size
313 measurement (DOX-MI: $18\pm 4\%$ below CTRL-MI, $p=0.03$), heart/body weight and heart
314 weight/tibia length ratios (Figure 3B-C). *In vivo* heart function was investigated using
315 echocardiography (Figure 3D). Compared to CTRL-treated *Rosa26-RTTA/Tet(O)-Fgf10*
316 infarcted mice, DOX-treated *Rosa26-RTTA/Tet(O)-Fgf10* infarcted mice displayed preserved
317 cardiac function and remodeling parameters including ejection fraction, fractional shortening
318 and left ventricular dilation (Figure 3E-G). Analysis of key heart failure markers using qRT-PCR
319 experiments confirmed the reduction of pathological remodeling in DOX-treated *Rosa26-*
320 *RTTA/Tet(O)-Fgf10* infarcted mice compared to CTRL-treated *Rosa26-RTTA/Tet(O)-Fgf10*
321 infarcted mice (Figure 3H). To confirm the specificity of the protective effect of FGF10 post-
322 MI, *Rosa26-RTTA* transgenic mice were subjected to MI and treated with DOX-supplemented
323 or CTRL food one day after MI during 21 days (Supplemental Figure 3A). qRT-PCR experiments
324 performed on left ventricular tissues 21 days post-MI confirmed that DOX-treatment has no
325 impact on myocardial *Fgf10* expression ($FC=0.9\pm 0.2$, $p=0.2$, CTRL-*Rosa26-RTTA*-MI, DOX-
326 *Rosa26-RTTA*-MI, $n=4$ per group). Similarly, no improvement in *in vivo* heart function was
327 observed 21 days post-MI. Cardiac function and remodeling of the DOX-treated *Rosa26-RTTA*-
328 MI mice were comparable to that of CTRL-treated *Rosa26-RTTA*-MI mice (Supplemental Figure
329 3), attesting to the positive effect of *Fgf10* upregulation in preserving cardiac function and
330 reducing remodeling post-MI.

331

332 **3.5 *Fgf10* upregulation following MI promotes cardiomyocyte renewal and prevents** 333 **myocardial necrosis and fibrosis**

334 To determine if endogenous *Fgf10* upregulation post-MI promotes cardiomyocyte renewal,
335 cardiac cell proliferation was analyzed in the BZ and IA of CTRL- and DOX-treated *R26R-*

336 *RTTA/Tet(O)-Fgf10*-MI hearts 5 (MI-5d) and 21 (MI-21d) days after injury (Figure 4A).
337 Immunofluorescence analysis of the proliferative capacities using Ki67 (Figure 4B-D
338 and Supplemental Figure 4A), PH3 (Supplemental Figure 4B-C) and Aurora kinase B (AURKB,
339 Figure 4E) revealed that upregulated *Fgf10* levels post-MI significantly enhances
340 cardiomyocyte renewal in both IA and BZ. Interestingly, while *Fgf10* upregulation
341 post-MI enhances cardiomyocyte renewal, it has no impact or even reduces
342 proliferation of non-myocytes (Supplemental Figure 4D-E). This observed increase in
343 cardiomyocyte cell cycle is specifically due to *Fgf10* upregulation since no change in the level
344 of Ki67⁺- or PH3⁺-cardiomyocytes could be detected in DOX-*Rosa26-RTTA* compared to
345 CTRL-*R26R-RTTA/Tet(O)-Fgf10* treated MI hearts (Supplemental Figure 4F-H). Analysis of
346 cardiomyocyte cross-sectional area frequency within the injured ventricle revealed a
347 significant upregulation of small cardiomyocytes in the BZ and IA of DOX- compared to CTRL-
348 treated *R26R-RTTA/Tet(O)-Fgf10*-MI hearts (Figure 4F). This observation is consistent with
349 the presence of newly formed cardiomyocytes following upregulation of FGF10 post-MI.
350 Newly formed cardiomyocytes have been shown to arise from a rare proliferative
351 subpopulation of mononucleated cardiomyocytes (17-19). We evaluated the impact of
352 increased *Fgf10* levels on cardiomyocyte nucleation in pathological conditions using
353 isolated cardiomyocytes from CTRL- and DOX-treated *R26R-RTTA/Tet(O)-Fgf10* hearts
354 (Figure 4G-J). Our results demonstrated that after MI elevated FGF10 levels
355 increased mononucleated cardiomyocyte numbers (Figure 4H-I). Immunofluorescence
356 analysis of proliferative capacity using Ki67 revealed that FGF10 significantly
357 enhances Ki67⁺-mononucleated cardiomyocyte numbers post-MI (Figure 4J). Similar results
358 were observed in normal conditions (Supplemental Figure 5A-D). To a lesser extent, FGF10
359 also increases Ki67⁺-binucleated cardiomyocyte numbers (Supplemental Figure 5E). Finally,
lineage tracing analysis using *aMHC-MerCreMer/R26R-tdT-RTTA/Tet(O)-Fgf10* mice
confirmed the hypothesis that 15

360 the newly formed cardiomyocytes derived from pre-existing cardiomyocytes ([Supplemental](#)
361 [Figure 5A and F](#); 8159 counted cardiomyocytes, 100% MF20⁺Tomato⁺, n=9).

362 Myocardial infarction results in massive cardiomyocyte necrosis that leads to the release of
363 myocardial biochemical markers, including Troponin T and I, in circulating blood (20). To
364 address whether *Fgf10* upregulation post-MI affects cardiomyocyte necrosis, serum contents
365 of cardiac troponin T (cTnT) and I (cTnI) were determined in CTRL- and DOX-MI mice
366 ([Supplemental Figure 6A](#)). Our results revealed that both cTnT ([Supplemental Figure 6B](#)) and
367 cTnI ([Supplemental Figure 6C](#)) serum levels were significantly reduced in DOX- compare to
368 CTRL-treated MI mice suggesting that, in addition to promoting cardiomyocyte renewal,
369 FGF10 prevents cardiomyocyte necrosis post-MI.

370 We then investigated the impact of *Fgf10* upregulation post-MI on cardiac fibrosis.
371 Histological analysis using Sirius red staining and qRT-PCR analysis were performed. Decreased
372 fibrosis was observed in DOX-treated *R26R-RTTA/Tet(O)-Fgf10*-MI hearts 21 days post-MI,
373 compared to CTRL-treated *R26R-RTTA/Tet(O)-Fgf10*-MI hearts ([Figure 4K-L](#)). This was
374 accompanied by downregulated collagen gene expression ([Figure 4M](#)). Finally, *in vitro*
375 experiments using human cardiac fibroblasts demonstrated that FGF10 is able to significantly
376 reduce TGF- β 1-induced cardiac fibroblast activation into α -SMA (*Acta2*)-expressing
377 myofibroblasts ([Figure 4N](#)), suggesting that FGF10 may play an upstream role in preventing
378 fibrosis post-MI.

379

380 **3.6 Molecular mechanisms underlying FGF10-induced cardiac regeneration and repair**

381 To uncover the molecular mechanisms by which FGF10 promotes cardiac regeneration and
382 repair following MI, genome wide transcriptomic analysis was performed by RNA-seq on IA
383 from CTRL- and DOX-treated *Rosa26-RTTA/Tet(O)-Fgf10* 21 days post-injury ([Figure 5](#)).

384 Unsupervised clustering of the normalized expression values of the differentially expressed
385 genes (DEG) strictly segregates DOX- from CTRL-treated *Rosa26-RTTA/Tet(O)-Fgf10* IA (Figure
386 5A). Among the 2016 DEG ($\text{Log}_2\text{FC} > 0.5$; adjusted p-value < 0.05), 831 were downregulated in
387 DOX-*Rosa26-RTTA/Tet(O)-Fgf10*, and expression of 1185 genes was increased compared with
388 CTRL-*Rosa26-RTTA/Tet(O)-Fgf10* (Figure 5B, Supplemental Table 1). As an internal control, we
389 detected significant upregulation of *Fgf10* transcripts ($\text{Log}_2\text{FC} = 5.4$, adjusted p-value $= 6 \times 10^{-7}$).
390 Consistent with the activation of cardiac regenerative and repair processes, gene ontology
391 enrichment analysis (Figure 5C) identified categories including heart process, developmental
392 process, mitochondria, extracellular matrix and immune process. Myocardial infarction is
393 associated with an early inflammatory response, which is a prerequisite for healing and scar
394 formation (21). Since our RNAseq was performed 21 days post-MI, we thus evaluated a
395 potential role for FGF10 in modulating myocardial levels of inflammatory cytokines and
396 immune cell recruitment 5 days post-myocardial infarction. Myocardial expression analysis of
397 key inflammatory cytokines and immune cell markers (monocytes and macrophages) was
398 performed in CTRL- and DOX-treated *R26R-RTTA/Tet(O)-Fgf10*-MI hearts (Supplemental
399 Figure 7A-C) and in WT- and *Fgf10*^{+/-}-MI hearts (Supplemental Figure 7D-F), nevertheless, no
400 change in selected marker expression was detected. In addition to significant downregulation
401 of genes involved in extracellular matrix remodeling, cardiac fibroblast markers including *Ddr2*
402 and *Pdgfra* display reduced expression (Figure 5E), consistent with reduced fibrosis in DOX-
403 versus CTRL-treated *Rosa26-RTTA/Tet(O)-Fgf10* hearts post-MI (Figure 4K-M) and our
404 experiments using human cardiac fibroblast cultures suggesting that FGF10 may play an
405 upstream role in preventing fibrosis post-MI (Figure 4N).

406 KEGG pathway annotation analysis (Figure 5D) revealed critical signaling pathways
407 overrepresented among selected DEG, including known downstream FGF10 signaling

408 cascades such as the MAPK, PI3K and FOXO pathways. Consistent with the impact of
409 FGF10 on the activation of cardiomyocyte cell cycle reentry, multiple genes related to
410 cell cycle modulation, including downregulated expression of a gene that negatively
411 regulates cardiomyocyte cell cycle, *Meis1* (18, 22), were identified (Figure 5E).

412 Metabolic pathways were also identified as overrepresented. FGF10 is known to
413 potentiate, through the activation of the PI3K/AKT/mTOR pathway, HIF1 α translation
414 (23) which expression stabilization favors glycolytic metabolism (24). We found that
415 increased *Fgf10* levels post-MI activate the PI3K pathway, including transcriptional
416 upregulation of the mTOR gene, and significantly enhance HIF1 α downstream target
417 expression including glycolysis-related genes (Figure 5E). Our data thus demonstrate that
418 *Fgf10* upregulation post-MI favors a strong metabolic switch towards glycolysis. As described
419 in other tissues (24), the observed upregulation of the AMPK/fatty acid signaling cascade is
420 consistent with the completion of the regenerative process ensuring re-differentiation of
421 newly formed contractile cardiomyocytes. The Hippo pathway has been recently described
422 to be a critical determinant for promoting adult cardiomyocyte cell cycle reentry (25). Our
423 data revealed that enhanced *Fgf10* levels post-MI leads to the transcriptional activation
424 of multiple key components of the Hippo pathway, including *Park2*, which has recently
425 been shown to play an essential role in Hippo-induced heart repair and regeneration (26)
426 (Figure 5E).

427 To confirm the crucial role of FGF10 in promoting the activation of signaling and cellular
428 events required to promote cardiomyocyte cell cycle reentry, we evaluated the impact of
429 decreased *Fgf10* dosage on the expression of genes encoding key glycolytic enzymes (*Pdk2*
430 and *Eno3*), the transcription factor *Meis1* and the Hippo pathway member *Park2*, 21
431 days after myocardial infarction. Our results demonstrate that, compared to WT-MI hearts,
Fgf10^{+/-}-MI

431 hearts display significantly reduced *Pdk2* and *Eno3* and *Park2* expression levels,
432 whereas *Meis1* expression is enhanced (Supplemental Figure 8).

433 Together these results suggest that FGF10 promotes cardiac regeneration by
434 modulating major regenerative pathways including the regulation of *Meis1* expression
435 levels, the Hippo signaling pathway and a pro-glycolytic metabolic switch.

436

437 **3.7 In failing human hearts, elevated *FGF10* expression correlates with high levels of** 438 **cardiomyocyte proliferation and reduced cardiac fibrosis**

439 We then investigated *FGF10* expression levels in failing explanted human heart samples
440 (Supplemental Table 2). Transcript levels were quantified by qRT-PCR in different
441 microdissected regions of explanted hearts. Our results revealed elevated *FGF10* levels in
442 the injured ventricles compared to right ventricular *FGF10* levels. Indeed 4 out of 7
443 hearts displayed increased *FGF10* expression in the BZ and 5 out of 7 hearts displayed
444 enhanced *FGF10* levels in the IA (Supplemental Figure 9A). We then evaluated
445 whether human ventricular *FGF10* levels may influence cardiomyocyte renewal.
446 Immunofluorescence experiments using Ki67 revealed that elevated *FGF10* levels
447 significantly correlate with enhanced Ki67⁺ cardiomyocyte numbers in the BZ (Figure 6A-
448 B) and the IA (Supplemental Figure 9B-C). In the BZ, cardiomyocyte cross-sectional area
449 measurement using WGA staining revealed that, except for heart sample B, elevated
450 *FGF10* levels correlate with decreased cardiomyocyte cell size (Figure 6E and Supplemental
451 Figure 9D-E). In addition, the analysis of cardiomyocyte size frequency Supplemental Figure
452 9F) demonstrated that elevated *FGF10* levels correlate with a high frequency of small
453 cardiomyocytes (<600 μm^2 , Figure 6C) and with a low frequency of large cardiomyocytes
454 (>800 μm^2 , Supplemental Figure 9G), suggesting that, consistent with our results in mice,
higher *FGF10* levels in human hearts favors cardiomyocyte

455 renewal. Despite low *FGF10* expression levels in the BZ of patient B, a high frequency of small
456 cardiomyocytes are observed in that area. This unexpected result may be explained by the
457 high level of *FGF10* expression in the IA that may influence cardiomyocyte status in the
458 adjacent BZ. Finally, to determine whether human myocardial *FGF10* levels influence cardiac
459 fibrosis, histological analysis using Sirius red staining was performed and fibrosis was
460 quantified. Our results demonstrated that elevated *FGF10* levels strongly correlate with
461 reduced fibrosis in the IA (Figure 6D and F) and the BZ (Supplemental Figure 9H-I).
462 These results obtained in human heart samples reinforce the conclusions of our mouse
463 experiments and support the relevance for FGF10 in promoting cardiomyocyte renewal
464 and preventing fibrosis.

465 **4. DISCUSSION**

466

467 In this study, we demonstrated that *Fgf10* expression post-MI promotes cardiac
468 regeneration and repair through two cellular mechanisms: elevating cardiomyocyte
469 renewal and limiting fibrosis. Our results suggest that FGF10 activates major regenerative
470 pathways including the regulation of *Meis1* expression levels, the Hippo signaling
471 pathway and a pro-glycolytic metabolic switch as well as playing a direct role in preventing
472 cardiac myofibroblast activation. Moreover, elevated *FGF10* levels in failing explanted
473 human heart samples strongly correlate with enhanced cardiomyocyte proliferation and
474 reduced fibrosis. Together our study highlights the pro-regenerative capacities of FGF10
475 and supports FGF10 as a clinically relevant target for heart regeneration in man.

476 After birth, the vast majority of cardiomyocytes undergo maturation leading to
477 multinucleation and metabolic switch toward oxidative phosphorylation (27,
478 28). Nevertheless, a rare population of resident adult mononucleated cardiomyocytes,
479 generally smaller than binucleated cardiomyocytes, has been described to participate to
480 cardiomyocyte renewal in normal aging (17, 19, 22, 29). We demonstrated that FGF10
481 enhances adult mononucleated cardiomyocyte numbers by promoting cell division of
482 pre-existing adult mononucleated cardiomyocytes. However, since cytokinesis of
483 binucleated cardiomyocytes is also possible (14), we cannot exclude that FGF10
484 may also promote binucleated cardiomyocyte cell division.

485 Cardiomyocyte metabolic reprogramming toward glycolysis, has been recently reported to be
486 required for cardiac regeneration (30). Our data indicate that, through the activation of
487 the mTOR/HIF1 α pathway activation, FGF10 post-MI favors a glycolytic metabolic switch.

FGF-

488 dependent control of c-MYC expression that, in turn, regulates expression of glycolytic
489 enzymes may also participate in the glycolytic metabolic switch (31).

490 Our results suggest that signaling events downstream of FGF10 may negatively regulate
491 *Meis1*, allowing the removal of a cell cycle block leading to cardiomyocyte cell cycle reentry
492 and cardiac regeneration. The transcription factor MEIS1 participates in postnatal
493 cardiomyocyte cell cycle exit through the activation of cyclin-dependent kinase inhibitor
494 expression and *Meis1* deletion in cardiomyocytes is sufficient to promote cardiomyocyte
495 mitosis in the adult heart (22). Interestingly, the rare proliferative adult cardiomyocyte
496 population is highly hypoxic (Hif1 α -responsive) and displays decreased *Meis* family member
497 gene expression (18).

498 The release of the Hippo block operating in mature cardiomyocytes seems to be a crucial
499 checkpoint to enable cardiomyocytes to reenter the cell cycle and the modulation of Hippo
500 pathway components critically participates in cardiac regeneration (25). Our study
501 demonstrated significantly upregulated levels of the Hippo pathway downstream target *Park2*
502 in *Fgf10*-overexpressing hearts. The ubiquitin ligase Parkin, encoded by the *Park2* gene, plays
503 an essential role in normal postnatal cardiac mitochondrial and metabolic maturation by
504 promoting mitophagy (32). *Park2* was also reported to play a critical role in the adaptive
505 response after MI by promoting clearance of damaged mitochondria via autophagy (33).
506 Recently, Leach *et al.*, revealed that *Park2* is essential for the Hippo-induced heart
507 regeneration (26). In our study, *Park2* may thus also participate to the metabolic switch in
508 response to forced *Fgf10* expression.

509 Decreased cardiomyocyte cell size has been shown to be an indicator of enhanced
510 cardiomyocyte proliferation (17, 19, 22, 29). Our results demonstrating that FGF10
511 significantly increases the number of small cardiomyocyte in the injured ventricle strongly

512 supports FGF10-induced cardiomyocyte renewal. Cardiomyocyte cell size is nevertheless
513 controlled by a balance between atrophic and hypertrophic signaling (34). Here, a role of
514 FGF10 on the modulation of atrophic gene expression cannot be excluded. Indeed, among
515 diverse genes described to regulate cardiac atrophy, we identified that FGF10 overexpression
516 21 days post-MI significantly upregulates *Murf1* transcript levels ($\text{Log}_2\text{FC}=2.7$, adjusted p-
517 value=0.003).

518 In addition to promoting cardiomyocyte renewal, our data suggest that FGF10 exposure
519 significantly decreases cardiac myofibroblast activation. Of particular interest, *Fgf10*-
520 overexpression post-MI results in the significant downregulation of *Smoc1* and *Smoc2*,
521 silencing of which has been recently shown to be required to prevent myofibroblast
522 transformation (35, 36). Here, we cannot exclude a role for FGF10 in epicardial priming
523 required for neovascularization (37) and the secretion of pro-regenerative signals in
524 pathological conditions (38). Furthermore, FGF10 anti-inflammatory properties (39, 40)
525 may potentially participate in the regenerative process induced by FGF10 treatment.

526 Alternatively, or in addition, the ability of FGF10 to promote functional cardiomyocyte
527 differentiation during ESC/iPSC differentiation (41) and cardiac reprogramming (42), may
528 also participate in the observed FGF10-induced cardioprotective effect.

529 In addition to ischemic-related pathologies, the therapeutic effect of FGF10 has been
530 extensively studied in wound healing, venous ulcers, mucositis, or ulcerative colitis, leading to
531 early human clinical studies clearly demonstrating FGF10 clinical safety and thus supporting
532 its utilization in clinics (43, 44). The fact that in human terminal heart failure, elevated
533 myocardial *FGF10* levels associate with enhanced cardiomyocyte proliferative capacities and
534 reduced fibrosis reinforces our results obtained in mice. In contrast to mouse models, few
535 experiments have addressed the capacity of human cardiomyocytes to respond to

536 regenerative signals (45, 46). Our results identify FGF10 as a potential regulator of
537 cardiomyocyte cell cycle and fibrosis in the adult human heart.

538 Together, our results indicate that FGF10 preserves cardiac remodeling and performance of
539 the injured heart, strongly supporting FGF10 as a clinical relevant target to promote cardiac
540 regeneration and repair in human patients.

541

542 DATA AVAILABILITY

543

544 The data underlying this article are available in the article and in its online [supplementary](#)
545 [material](#).

546

547 FUNDING

548

549 This work was supported by the Agence Nationale de la Recherche grant ANR-14-CE12-12-02,
550 the Fédération Française de Cardiologie, and AFM-Téléthon grant no. 20777 awarded to FR
551 and an AFM-Téléthon post-doctoral fellow awarded to FH.

552

553 ACKNOWLEDGEMENTS

554

555 We thank Valerie Delague, David Salgado and Laurent Argiro from the Genomics and
556 Bioinformatics Platform (GBiM) from the U 1251/Marseille Medical Genetics for supervising
557 and performing, respectively, the RNAseq experiments. We thank Regis Guieu (Laboratory of
558 Biochemistry, Timone Hospital) for advice on biochemical analysis. We thank Patrick Lechêne
559 (Inserm UMR-S 1180) for statistical advice. We are grateful to Rodolphe Fischmeister (Inserm
560 UMR-S 1180) for his comments and advice on the manuscript.

561

562 CONFLICT OF INTEREST

563

564 The authors have declared that no conflict of interest exists.

565

566 **REFERENCES**

- 567 1. Benjamin EJ, Virani SS, Callaway CW, Chamberlain AM, Chang AR, Cheng S, Chiuve SE, Cushman M,
568 Delling FN, Deo R, de Ferranti SD, Ferguson JF, Fornage M, Gillespie C, Isasi CR, Jimenez MC, Jordan
569 LC, Judd SE, Lackland D, Lichtman JH, Lisabeth L, Liu S, Longenecker CT, Lutsey PL, Mackey JS,
570 Matchar DB, Matsushita K, Mussolino ME, Nasir K, O'Flaherty M, Palaniappan LP, Pandey A, Pandey
571 DK, Reeves MJ, Ritchey MD, Rodriguez CJ, Roth GA, Rosamond WD, Sampson UKA, Satou GM, Shah
572 SH, Spartano NL, Tirschwell DL, Tsao CW, Voeks JH, Willey JZ, Wilkins JT, Wu JH, Alger HM, Wong
573 SS, Muntner P, American Heart Association Council on E, Prevention Statistics C, and Stroke
574 Statistics S. Heart Disease and Stroke Statistics-2018 Update: A Report From the American Heart
575 Association. *Circulation*. 2018;137(12):e67-e492.
- 576 2. Bergmann O, Bhardwaj RD, Bernard S, Zdunek S, Barnabe-Heider F, Walsh S, Zupicich J, Alkass K,
577 Buchholz BA, Druid H, Jovinge S, and Frisen J. Evidence for cardiomyocyte renewal in humans.
578 *Science*. 2009;324(5923):98-102.
- 579 3. Eschenhagen T, Bolli R, Braun T, Field LJ, Fleischmann BK, Frisen J, Giacca M, Hare JM, Houser S, Lee
580 RT, Marban E, Martin JF, Molkentin JD, Murry CE, Riley PR, Ruiz-Lozano P, Sadek HA, Sussman MA,
581 and Hill JA. Cardiomyocyte Regeneration: A Consensus Statement. *Circulation*. 2017;136(7):680-6.
- 582 4. Tzahor E, and Poss KD. Cardiac regeneration strategies: Staying young at heart. *Science*.
583 2017;356(6342):1035-9.
- 584 5. Payan SM, Hubert F, and Rochais F. Cardiomyocyte proliferation, a target for cardiac regeneration.
585 *Biochim Biophys Acta Mol Cell Res*. 2019.
- 586 6. Hortells L, Johansen AKZ, and Yutzey KE. Cardiac Fibroblasts and the Extracellular Matrix in
587 Regenerative and Nonregenerative Hearts. *J Cardiovasc Dev Dis*. 2019;6(3).
- 588 7. Rochais F, Sturny R, Chao CM, Mesbah K, Bennett M, Mohun TJ, Bellusci S, and Kelly RG. FGF10
589 promotes regional foetal cardiomyocyte proliferation and adult cardiomyocyte cell-cycle re-entry.
590 *Cardiovasc Res*. 2014;104(3):432-42.

- 591 8. Itoh N, Ohta H, Nakayama Y, and Konishi M. Roles of FGF Signals in Heart Development, Health, and
592 Disease. *Front Cell Dev Biol.* 2016;4(110).
- 593 9. Hubert F, Payan SM, and Rochais F. FGF10 Signaling in Heart Development, Homeostasis, Disease
594 and Repair. *Front Genet.* 2018;9(599).
- 595 10. Marguerie A, Bajolle F, Zaffran S, Brown NA, Dickson C, Buckingham ME, and Kelly RG. Congenital
596 heart defects in *Fgfr2-IIIb* and *Fgf10* mutant mice. *Cardiovasc Res.* 2006;71(1):50-60.
- 597 11. Takagawa J, Zhang Y, Wong ML, Sievers RE, Kapasi NK, Wang Y, Yeghiazarians Y, Lee RJ, Grossman
598 W, and Springer ML. Myocardial infarct size measurement in the mouse chronic infarction model:
599 comparison of area- and length-based approaches. *J Appl Physiol (1985).* 2007;102(6):2104-11.
- 600 12. Watanabe Y, Zaffran S, Kuroiwa A, Higuchi H, Ogura T, Harvey RP, Kelly RG, and Buckingham M.
601 Fibroblast growth factor 10 gene regulation in the second heart field by *Tbx1*, *Nkx2-5*, and *Islet1*
602 reveals a genetic switch for down-regulation in the myocardium. *Proc Natl Acad Sci U S A.*
603 2012;109(45):18273-80.
- 604 13. Eulalio A, Mano M, Dal Ferro M, Zentilin L, Sinagra G, Zacchigna S, and Giacca M. Functional
605 screening identifies miRNAs inducing cardiac regeneration. *Nature.* 2012;492(7429):376-81.
- 606 14. D'Uva G, Aharonov A, Lauriola M, Kain D, Yahalom-Ronen Y, Carvalho S, Weisinger K, Bassat E,
607 Rajchman D, Yifa O, Lysenko M, Konfino T, Hegesh J, Brenner O, Neeman M, Yarden Y, Leor J, Sarig
608 R, Harvey RP, and Tzahor E. ERBB2 triggers mammalian heart regeneration by promoting
609 cardiomyocyte dedifferentiation and proliferation. *Nat Cell Biol.* 2015;17(5):627-38.
- 610 15. Jopling C, Sleep E, Raya M, Marti M, Raya A, and Izpisua Belmonte JC. Zebrafish heart regeneration
611 occurs by cardiomyocyte dedifferentiation and proliferation. *Nature.* 2010;464(7288):606-9.
- 612 16. Zhang Y, Li S, Yuan L, Tian Y, Weidenfeld J, Yang J, Liu F, Chokas AL, and Morrissey EE. *Foxp1*
613 coordinates cardiomyocyte proliferation through both cell-autonomous and nonautonomous
614 mechanisms. *Genes Dev.* 2010;24(16):1746-57.
- 615 17. Patterson M, Barske L, Van Handel B, Rau CD, Gan P, Sharma A, Parikh S, Denholtz M, Huang Y,
616 Yamaguchi Y, Shen H, Allayee H, Crump JG, Force TI, Lien CL, Makita T, Lusic AJ, Kumar SR, and Sucov

- 617 HM. Frequency of mononuclear diploid cardiomyocytes underlies natural variation in heart
618 regeneration. *Nature genetics*. 2017;49(9):1346-53.
- 619 18. Kimura W, Xiao F, Canseco DC, Muralidhar S, Thet S, Zhang HM, Abderrahman Y, Chen R, Garcia JA,
620 Shelton JM, Richardson JA, Ashour AM, Asaithamby A, Liang H, Xing C, Lu Z, Zhang CC, and Sadek
621 HA. Hypoxia fate mapping identifies cycling cardiomyocytes in the adult heart. *Nature*.
622 2015;523(7559):226-30.
- 623 19. Bersell K, Arab S, Haring B, and Kuhn B. Neuregulin1/ErbB4 signaling induces cardiomyocyte
624 proliferation and repair of heart injury. *Cell*. 2009;138(2):257-70.
- 625 20. Park KC, Gaze DC, Collinson PO, and Marber MS. Cardiac troponins: from myocardial infarction to
626 chronic disease. *Cardiovasc Res*. 2017;113(14):1708-18.
- 627 21. Frangiannis NG, Smith CW, and Entman ML. The inflammatory response in myocardial infarction.
628 *Cardiovasc Res*. 2002;53(1):31-47.
- 629 22. Mahmoud AI, Kocabas F, Muralidhar SA, Kimura W, Koura AS, Thet S, Porrello ER, and Sadek HA.
630 Meis1 regulates postnatal cardiomyocyte cell cycle arrest. *Nature*. 2013;497(7448):249-53.
- 631 23. Walker DJ, and Land SC. Regulation of vascular signalling by nuclear Sprouty2 in fetal lung epithelial
632 cells: Implications for co-ordinated airway and vascular branching in lung development. *Comp*
633 *Biochem Physiol B Biochem Mol Biol*. 2018;224(105-14).
- 634 24. Heber-Katz E. Oxygen, Metabolism, and Regeneration: Lessons from Mice. *Trends Mol Med*.
635 2017;23(11):1024-36.
- 636 25. Wang J, Liu S, Heallen T, and Martin JF. The Hippo pathway in the heart: pivotal roles in
637 development, disease, and regeneration. *Nat Rev Cardiol*. 2018;15(11):672-84.
- 638 26. Leach JP, Heallen T, Zhang M, Rahmani M, Morikawa Y, Hill MC, Segura A, Willerson JT, and Martin
639 JF. Hippo pathway deficiency reverses systolic heart failure after infarction. *Nature*.
640 2017;550(7675):260-4.
- 641 27. Soonpaa MH, Kim KK, Pajak L, Franklin M, and Field LJ. Cardiomyocyte DNA synthesis and
642 binucleation during murine development. *Am J Physiol*. 1996;271(5 Pt 2):H2183-9.

- 643 28. Piquereau J, and Ventura-Clapier R. Maturation of Cardiac Energy Metabolism During Perinatal
644 Development. *Front Physiol.* 2018;9(959).
- 645 29. Senyo SE, Steinhilber ML, Pizzimenti CL, Yang VK, Cai L, Wang M, Wu TD, Guerquin-Kern JL, Lechene
646 CP, and Lee RT. Mammalian heart renewal by pre-existing cardiomyocytes. *Nature.*
647 2013;493(7432):433-6.
- 648 30. Honkoop H, de Bakker DE, Aharonov A, Kruse F, Shakked A, Nguyen PD, de Heus C, Garric L, Muraro
649 MJ, Shoffner A, Tessadori F, Peterson JC, Noort W, Bertozzi A, Weidinger G, Posthuma G, Grun D,
650 van der Laarse WJ, Klumperman J, Jaspers RT, Poss KD, van Oudenaarden A, Tzahor E, and Bakkers
651 J. Single-cell analysis uncovers that metabolic reprogramming by ErbB2 signaling is essential for
652 cardiomyocyte proliferation in the regenerating heart. *Elife.* 2019;8(
- 653 31. Yu P, Wilhelm K, Dubrac A, Tung JK, Alves TC, Fang JS, Xie Y, Zhu J, Chen Z, De Smet F, Zhang J, Jin
654 SW, Sun L, Sun H, Kibbey RG, Hirschi KK, Hay N, Carmeliet P, Chittenden TW, Eichmann A, Potente
655 M, and Simons M. FGF-dependent metabolic control of vascular development. *Nature.*
656 2017;545(7653):224-8.
- 657 32. Gong G, Song M, Csordas G, Kelly DP, Matkovich SJ, and Dorn GW, 2nd. Parkin-mediated mitophagy
658 directs perinatal cardiac metabolic maturation in mice. *Science.* 2015;350(6265):aad2459.
- 659 33. Kubli DA, Zhang X, Lee Y, Hanna RA, Quinsay MN, Nguyen CK, Jimenez R, Petrosyan S, Murphy AN,
660 and Gustafsson AB. Parkin protein deficiency exacerbates cardiac injury and reduces survival
661 following myocardial infarction. *J Biol Chem.* 2013;288(2):915-26.
- 662 34. Razeghi P, and Taegtmeyer H. Hypertrophy and atrophy of the heart: the other side of remodeling.
663 *Ann N Y Acad Sci.* 2006;1080(110-9).
- 664 35. Gerarduzzi C, Kumar RK, Trivedi P, Ajay AK, Iyer A, Boswell S, Hutchinson JN, Waikar SS, and Vaidya
665 VS. Silencing SMOC2 ameliorates kidney fibrosis by inhibiting fibroblast to myofibroblast
666 transformation. *JCI Insight.* 2017;2(8).

- 667 36.Wang Y, and Wu X. SMOC1 silencing suppresses the angiotensin II-induced myocardial fibrosis of
668 mouse myocardial fibroblasts via affecting the BMP2/Smad pathway. *Oncol Lett.* 2018;16(3):2903-
669 10.
- 670 37.Vega-Hernandez M, Kovacs A, De Langhe S, and Ornitz DM. FGF10/FGFR2b signaling is essential for
671 cardiac fibroblast development and growth of the myocardium. *Development.* 2011;138(15):3331-
672 40.
- 673 38.Cao J, and Poss KD. The epicardium as a hub for heart regeneration. *Nat Rev Cardiol.*
674 2018;15(10):631-47.
- 675 39.Li YH, Fu HL, Tian ML, Wang YQ, Chen W, Cai LL, Zhou XH, and Yuan HB. Neuron-derived FGF10
676 ameliorates cerebral ischemia injury via inhibiting NF-kappaB-dependent neuroinflammation and
677 activating PI3K/Akt survival signaling pathway in mice. *Sci Rep.* 2016;6(19869).
- 678 40.Tan X, Zhu H, Tao Q, Guo L, Jiang T, Xu L, Yang R, Wei X, Wu J, Li X, and Zhang JS. FGF10 Protects
679 Against Renal Ischemia/Reperfusion Injury by Regulating Autophagy and Inflammatory Signaling.
680 *Front Genet.* 2018;9(556).
- 681 41.Chan SS, Li HJ, Hsueh YC, Lee DS, Chen JH, Hwang SM, Chen CY, Shih E, and Hsieh PC. Fibroblast
682 growth factor-10 promotes cardiomyocyte differentiation from embryonic and induced pluripotent
683 stem cells. *PLoS One.* 2010;5(12):e14414.
- 684 42.Yamakawa H, Muraoka N, Miyamoto K, Sadahiro T, Isomi M, Haginiwa S, Kojima H, Umei T, Akiyama
685 M, Kuishi Y, Kurokawa J, Furukawa T, Fukuda K, and Ieda M. Fibroblast Growth Factors and Vascular
686 Endothelial Growth Factor Promote Cardiac Reprogramming under Defined Conditions. *Stem Cell*
687 *Reports.* 2015;5(6):1128-42.
- 688 43.Beenken A, and Mohammadi M. The FGF family: biology, pathophysiology and therapy. *Nat Rev*
689 *Drug Discov.* 2009;8(3):235-53.
- 690 44.Plichta JK, and Radek KA. Sugar-coating wound repair: a review of FGF-10 and dermatan sulfate in
691 wound healing and their potential application in burn wounds. *J Burn Care Res.* 2012;33(3):299-
692 310.

- 693 45. Polizzotti BD, Ganapathy B, Walsh S, Choudhury S, Ammanamanchi N, Bennett DG, dos Remedios
694 CG, Haubner BJ, Penninger JM, and Kuhn B. Neuregulin stimulation of cardiomyocyte regeneration
695 in mice and human myocardium reveals a therapeutic window. *Sci Transl Med.*
696 2015;7(281):281ra45.
- 697 46. Canseco DC, Kimura W, Garg S, Mukherjee S, Bhattacharya S, Abdisalaam S, Das S, Asaithamby A,
698 Mammen PP, and Sadek HA. Human ventricular unloading induces cardiomyocyte proliferation. *J*
699 *Am Coll Cardiol.* 2015;65(9):892-900.

FIGURE LEGENDS

Figure 1: Decreased *Fgf10* dosage worsens cardiac function and remodeling following myocardial infarction. (A) Schematic of the experimental plan. WT and *Fgf10*^{+/-} adult mice were subjected to myocardial infarction (MI) and analysis were performed 21 days after surgery. (B) Heart weight/body weight ratio. WT-MI, n=26; *Fgf10*^{+/-}-MI, n=24. (C) Heart weight/tibia length ratio. WT-MI, n=20; *Fgf10*^{+/-}-MI, n=23. (D) M-mode images of echocardiographic experiments (Scale bars, x: 0.1 s; y: 1 mm). (E) Ejection fraction. (F) Fractional shortening. (G) Left ventricular systolic volume. WT-SHAM, n=14; *Fgf10*^{+/-}-SHAM, n=7; WT-MI, n=8; *Fgf10*^{+/-}-MI, n=6 (H) qRT-PCR analysis, on left ventricular tissues, of *Nppa* (n=5/group), *Nppb* (n=6/group) and *Myh7* (n=5-6/group) expression. *, p<0.05; **, 0,001<p<0.01; ***, p<0.001; Student's *t*-test.

Figure 2: Decreased *Fgf10* dosage impairs cardiomyocyte proliferation and worsens fibrosis following MI. (A) Schematic of the experimental plan. WT and *Fgf10*^{+/-} adult mice were subjected to myocardial infarction (MI) and analysis were performed 5 and 21 days after surgery. (B-D) Immunofluorescence experiments were performed to evaluate in the border zone *in vivo* cardiomyocyte proliferation (MF20⁺; yellow arrowheads) 5 days (C; MI-5d; WT, n=6; *Fgf10*^{+/-}, n=5) and 21 days (D; MI-21d; WT, n=5; *Fgf10*^{+/-}, n=6) post-MI using Ki67. (E) Immunofluorescence experiments using Aurora B marker were performed to evaluate *in vivo* cardiomyocyte proliferation (MF20⁺; yellow arrowheads) 5 days post-MI (n=6 mice/group). Scale bars, 10 μm (B) and 5 μm (E). (F) Cardiomyocyte cross-sectional area frequency (MI-21d; WT, n=6; *Fgf10*^{+/-}, n=5; compared using Fisher statistical test). (G-H) Histological sirius red staining was performed 5 days post-MI (WT, n=6; *Fgf10*^{+/-}, n=5, Scale bar, 1000 μm). (I) qRT-

PCR analysis 5 days post-MI of *Col1A1* (WT, n=5; *Fgf10*^{+/-}, n=7) and *Col3A1* (WT, n=6; *Fgf10*^{+/-}, n=6) expression in the border zone. (J-K) Histological sirius red staining was performed 21 days post-MI (WT, n=5; *Fgf10*^{+/-}, n=5, Scale bar, 1000 μ m). (L) qRT-PCR analysis 21 days post-MI of *Col1A1* (WT, n=7; *Fgf10*^{+/-}, n=5), *Col3A1* (WT, n=6; *Fgf10*^{+/-}, n=5) and *Col6A5* (WT, n=6; *Fgf10*^{+/-}, n=5) expression in the infarcted area. ns, non-significant; *, p<0.05; **, 0,001<p<0.01; ***, p<0.001; Student's *t*-test.

Figure 3: Upregulation of *Fgf10* levels post-MI preserves cardiac function and remodeling.

(A) Schematic of the experimental plan. *R26R-RTTA/Tet(O)-Fgf10* mice were subjected to myocardial infarction (MI). One day after MI, mice were fed with normal (CTRL) or doxycycline supplemented food (DOX) required to induce *Fgf10* overexpression and analyzed 21 days later. (B) Heart weight/body weight ratio. MI-CTRL, n=18; MI-DOX, n=25. (C) Heart weight/tibia length ratio. MI-CTRL, n=16; MI-DOX, n=25. (D) M-mode images of echocardiographic experiments (Scale bars, x: 0.1 s; y: 1 mm). (E) Ejection fraction. (F) Fractional shortening. (G) Left ventricular systolic volume. SHAM-CTRL, n=7; SHAM-DOX, n=6; MI-CTRL, n=12; MI-DOX, n=14. (H) qRT-PCR analysis, on left ventricular tissues, of *Nppa* (MI-CTRL, n=6; MI-DOX, n=7), *Nppb* (MI-CTRL, n=7; MI-DOX, n=7) and *Myh7* (MI-CTRL, n=6; MI-DOX, n=7) expression. ns, non-significant; *, p<0.05; **, 0,001<p<0.01; ***, p<0.001; Student's *t*-test.

Figure 4: Upregulation of *Fgf10* levels post-MI promotes cardiomyocyte cell cycle reentry and prevents fibrosis.

(A) Schematic of the experimental plan. *R26R-RTTA/Tet(O)-Fgf10* mice were subjected to myocardial infarction (MI). One day after MI, mice were fed with normal (CTRL) or doxycycline supplemented food (DOX) required to induce *Fgf10* overexpression and

analyzed 5 and 21 days later. (B-E) Immunofluorescence experiments were performed to evaluate, 5 (MI-5d) and 21 (MI-21d) days post-MI, in the border zone (BZ) and in the infarcted area (IA), cardiomyocyte (MF20⁺; yellow arrowheads) proliferation using Ki67⁺ (C, MI-5d; BZ CTRL n=5, BZ DOX n=5, IA CTRL n=5, IA DOX n=5 and D, MI-21d; BZ CTRL n=6, BZ DOX n=7, IA CTRL n=6, IA DOX n=6) and AURKB⁺ (E, n=5/group). (F) Cardiomyocyte cross-sectional area (n=6-7 mice/group). Scale bars, B: 10 μm; E: 5 μm and F: 25 μm. (G) *R26R-RTTA/Tet(O)-Fgf10* mice were subjected to myocardial infarction (MI). One day after MI, mice were fed with normal (CTRL) or doxycycline (DOX) supplemented food for 5 days. (H-J) Cardiomyocytes were isolated and immunofluorescence experiments were performed to evaluate mononucleated cardiomyocyte numbers (I) and their proliferative capacities (J); (n=5-6/group). (K-L) Fibrosis was investigated 21 days post-MI using histological sirius red staining. n=5/group. Scale bars, 1000 μm. (M) qRT-PCR analysis of *Col1A1* (n=6/group), *Col3A1* (n=6/group) and *Col6A5* (CTRL n=6 Dox n=7) expression in the infarcted area. (N) Human fibroblast cultures revealed that FGF10 prevents TGF-β1-induced fibroblast activation, (n=3/group). ns, non-significant; *, p<0.05; **, 0,001<p<0.01; ***, p<0,001; Student's *t*-test.

Figure 5: RNA-seq analysis reveals FGF10-induced transcriptional regulation of major regenerative pathways. *R26R-RTTA/Tet(O)-Fgf10* mice were subjected to myocardial infarction (MI). One day after MI, mice were fed with normal (CTRL) or doxycycline (DOX) supplemented food required to induce *Fgf10* overexpression. 21 days post-MI, RNA-seq analysis was performed in the infarcted area. (A) Heatmap showing hierarchical clustering of DEG in biological replicates (n=4/group). (B) Volcano plot of DEG sorted according to fold change and significance (FDR adjusted p-value). DEG (FDR < 0.05, n=2016) are shown in red, and non-significant changes are shown in black. (C) Enrichment analysis of gene ontology

terms for differentially regulated genes. Upregulated and downregulated genes in MI-DOX vs MI-CTRL are represented in red and blue, respectively. **(D)** Circular plot of 42 DEG showing the relationship between expression changes (left semicircle perimeter) and KEGG pathways (right semicircle perimeter). Changes in expression are represented for each gene as Log_2FC . **(E)** qRT-PCR experiments showing the validation of major candidate genes ($n=4-6/\text{group}$).

Figure 6: Upregulation of *FGF10* in human failing hearts correlates with increased cardiomyocyte proliferation, reduced cardiomyocyte size and reduced fibrosis. Human explanted failing heart samples from right ventricle (RV), remote area (RA), border zone (BZ) and infarcted area (IA) were collected from 7 patients (A-G). **(A)** Cardiomyocyte proliferation in the BZ was evaluated using immunofluorescence experiments and the cell cycle marker Ki67. **(B)** Elevated *FGF10* levels correlate with enhanced cardiomyocyte proliferation in the BZ. **(C)** Cardiomyocyte cross-sectional area was measured in the BZ using the cell membrane marker WGA. Elevated *FGF10* levels correlate with high frequency of small cardiomyocyte ($<600\mu\text{m}^2$). **(D)** Cardiac fibrosis in the IA was assessed using histological Sirius red staining. Elevated *FGF10* levels correlate with reduced fibrosis in the IA. **(E)** Representative pictures of WGA staining, according to patient-corresponding *FGF10* levels depicted in Supplemental Figure 8A, have been classified from low to high expression as represented by the above grey triangle. Scale bar 10 μm . **(E-F)** Representative pictures of Sirius red staining, according to patient-corresponding *FGF10* levels depicted in Supplemental Figure 8A, have been classified from low to high expression as represented by the above grey triangle. Scale bars 100 μm . Statistical significance (p) was determined using Student's t -distribution.

FIGURE 1

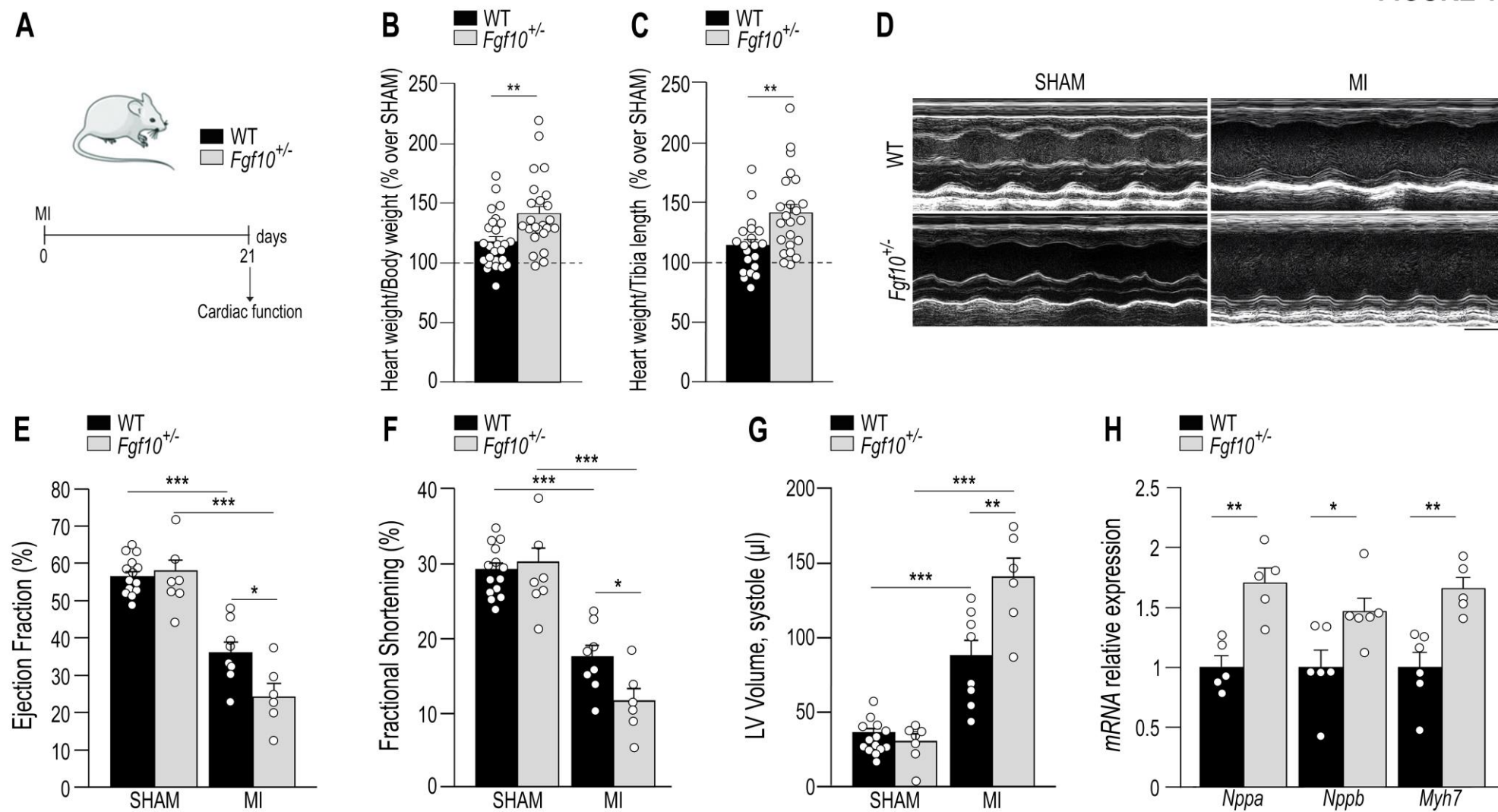


FIGURE 2

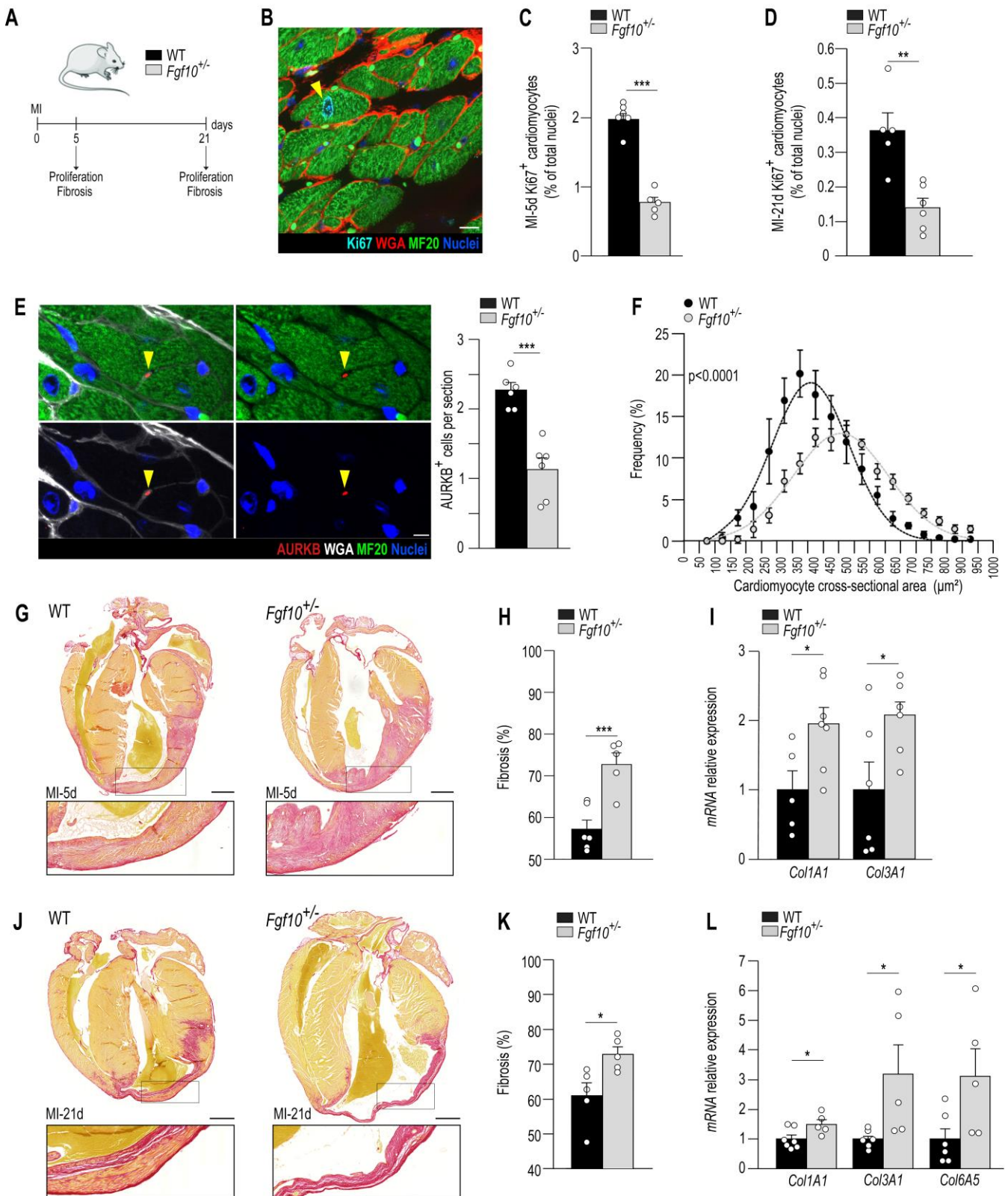


FIGURE 3

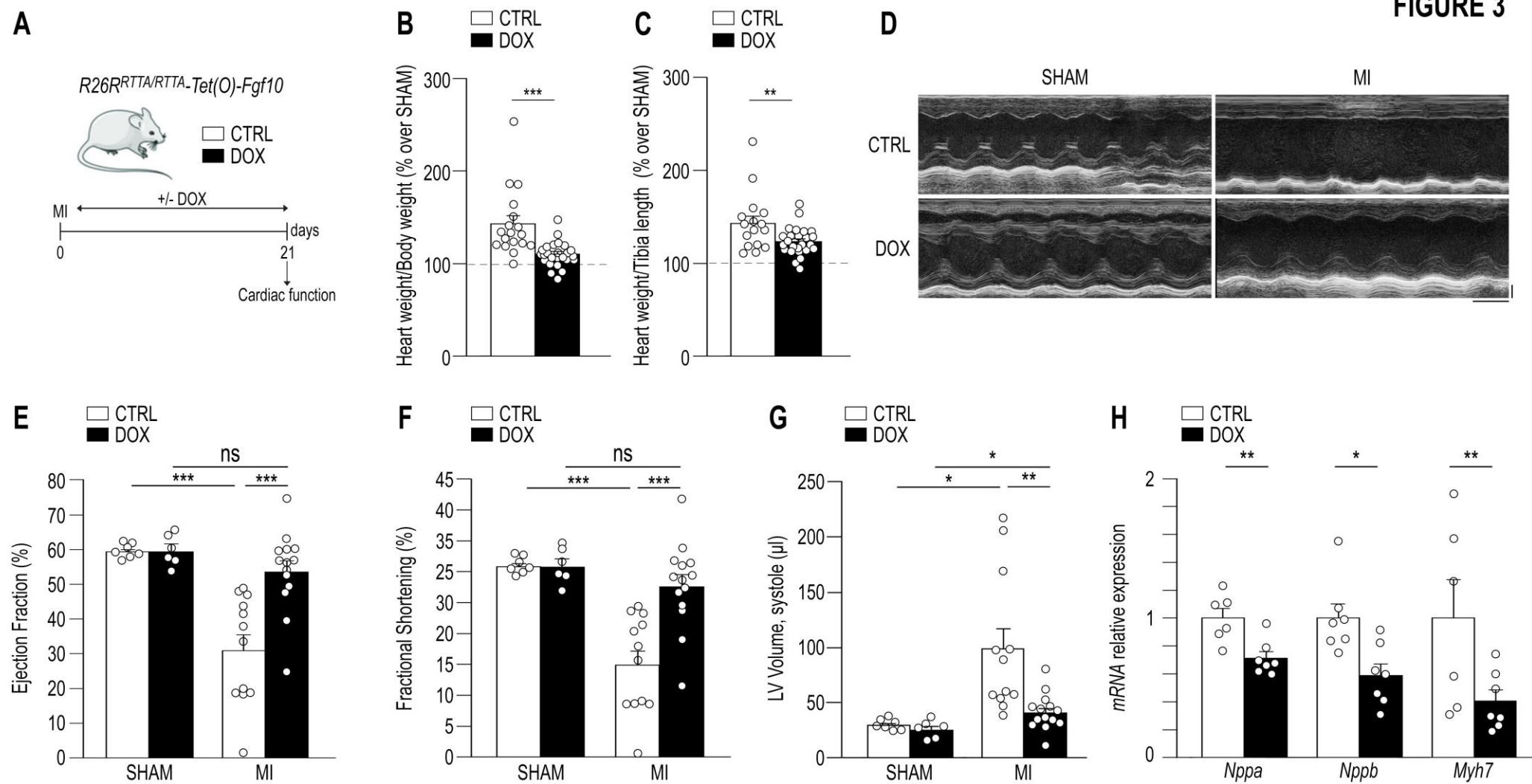


FIGURE 4

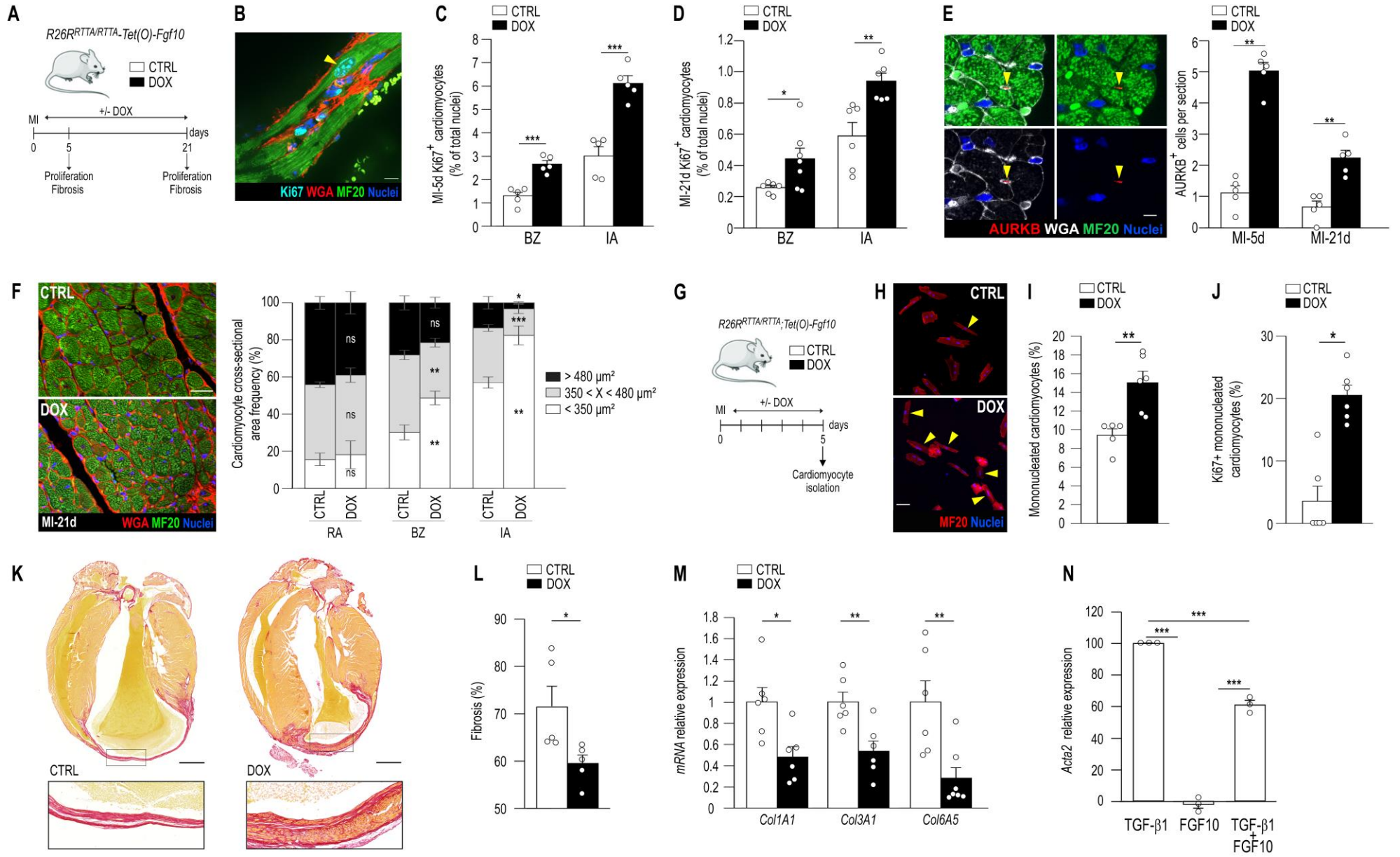


FIGURE 5

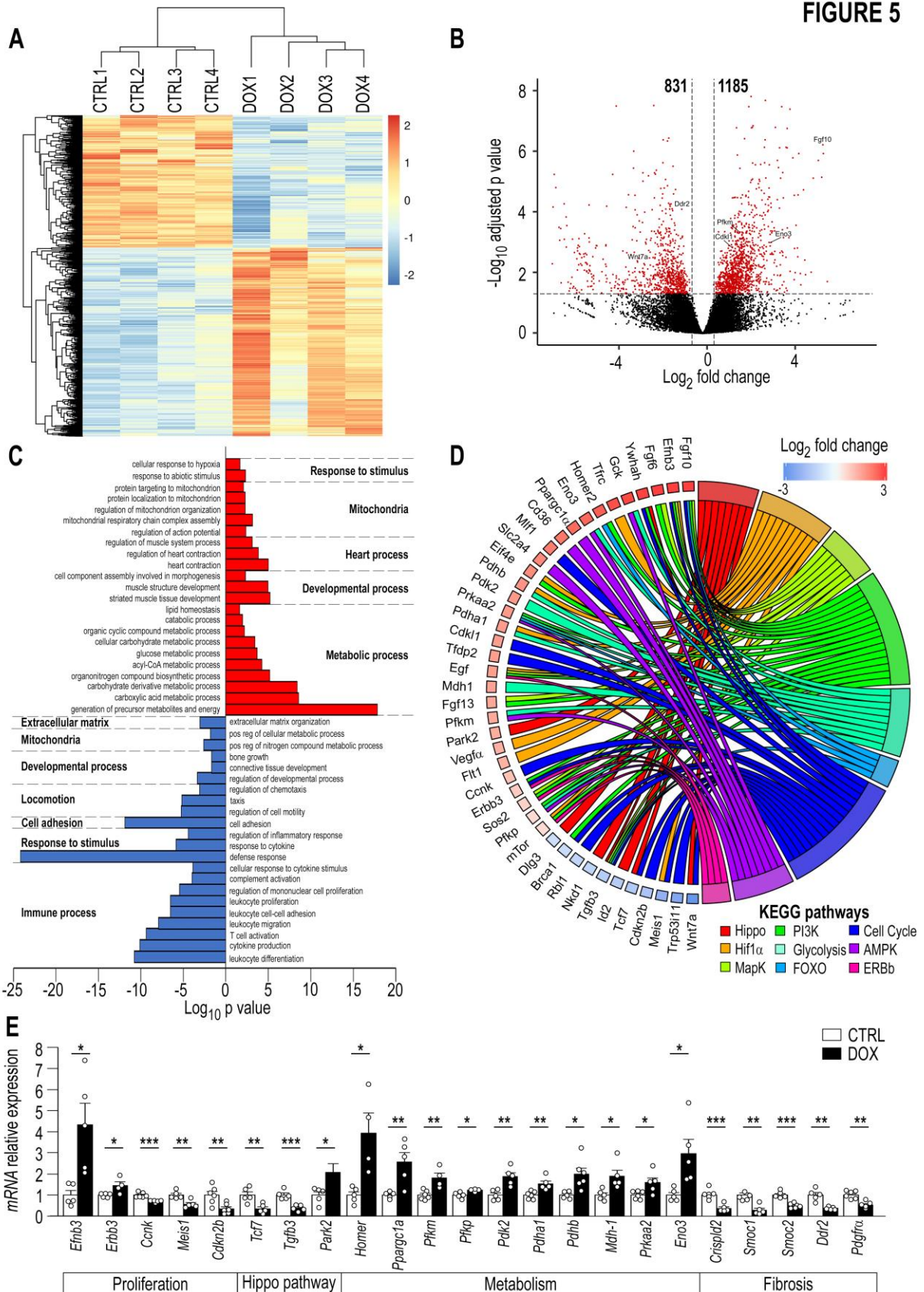
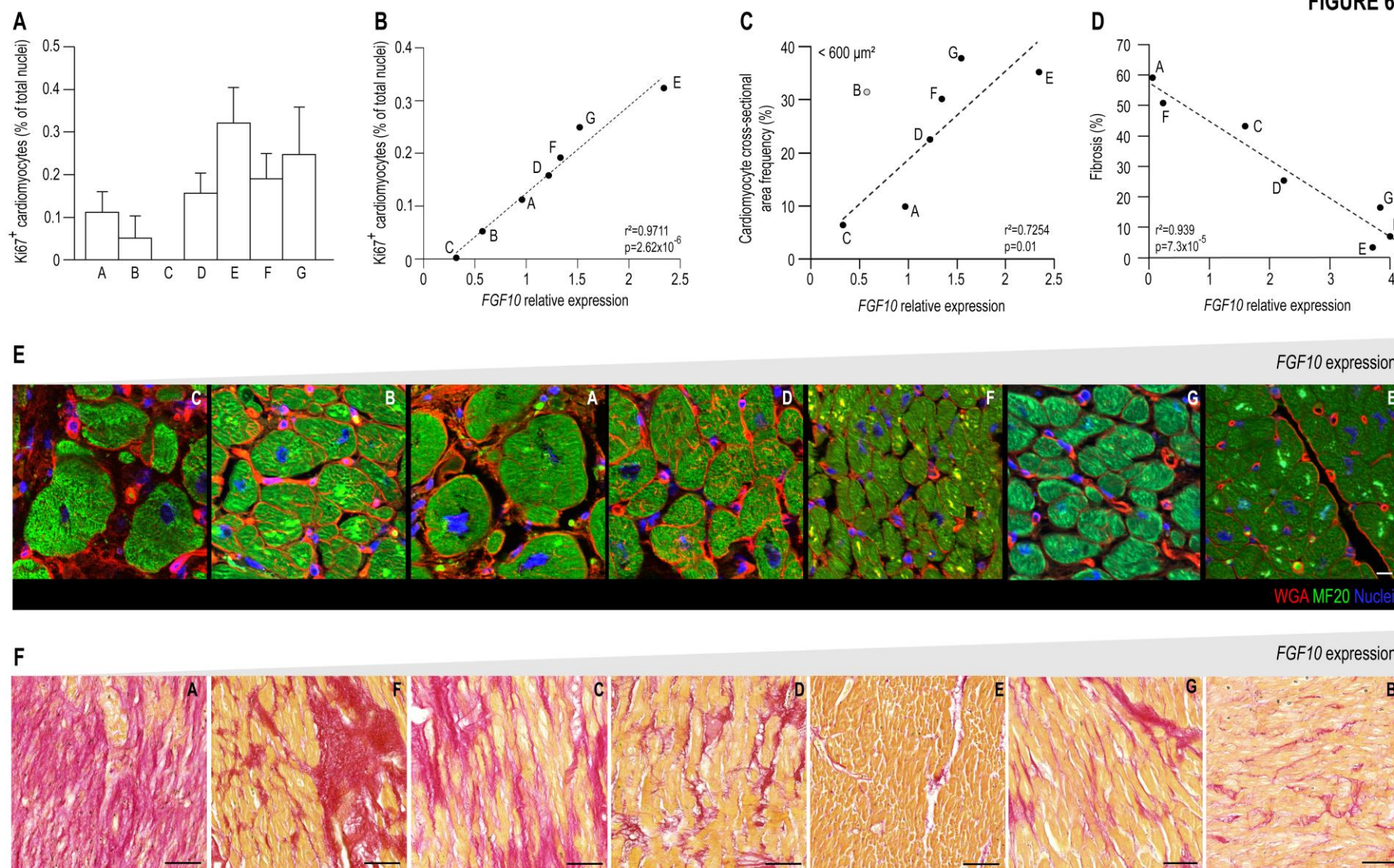
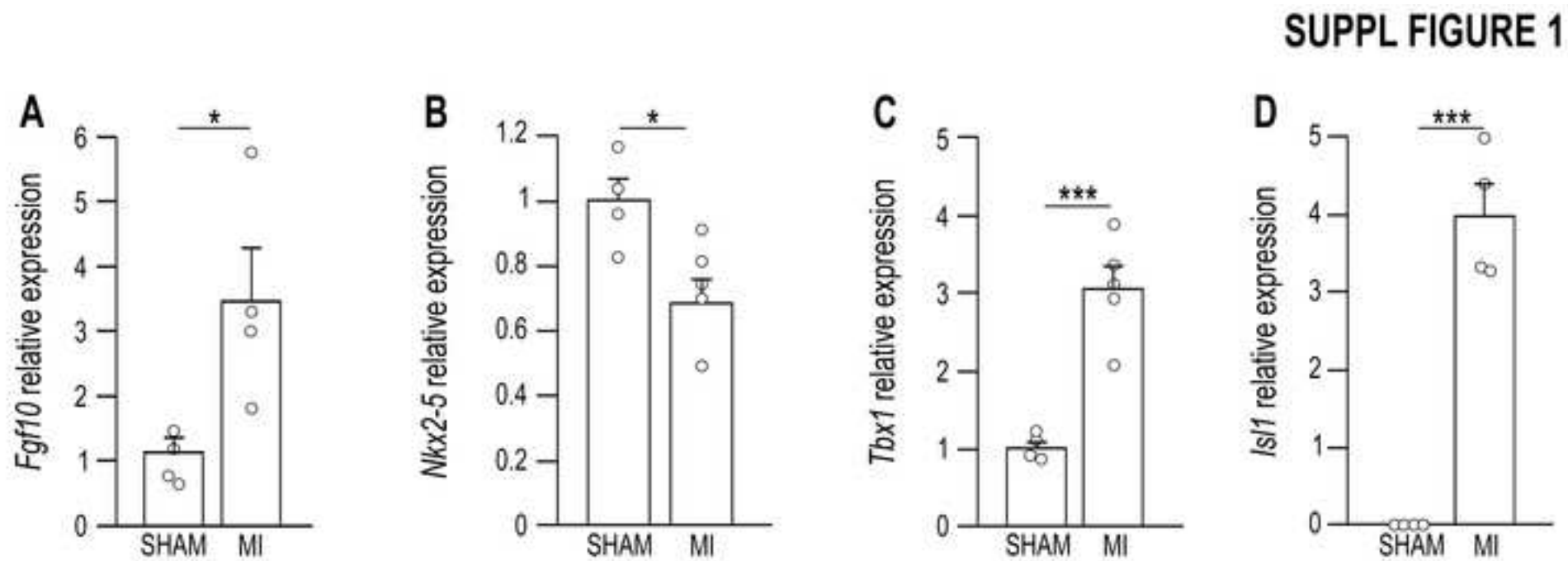
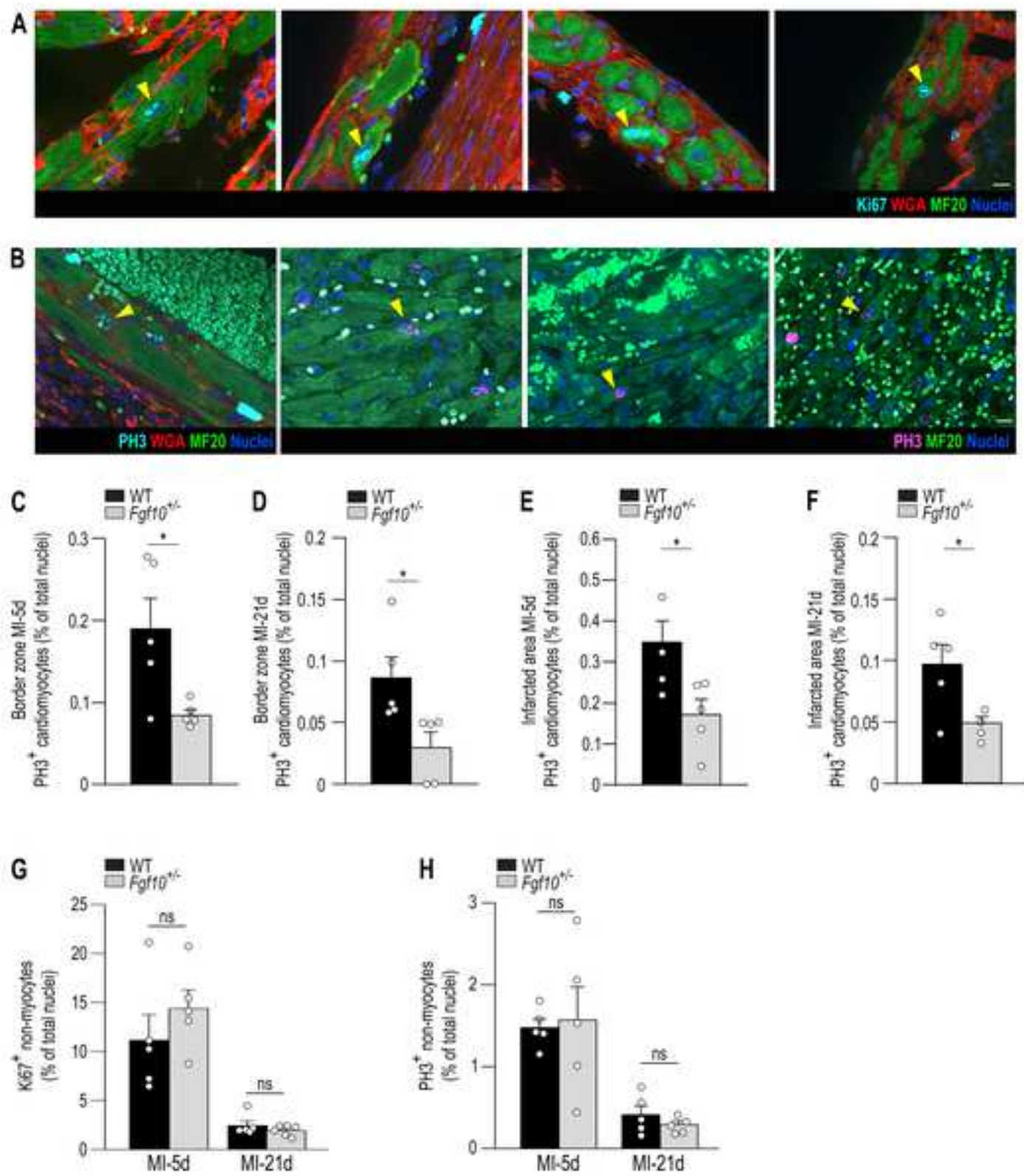


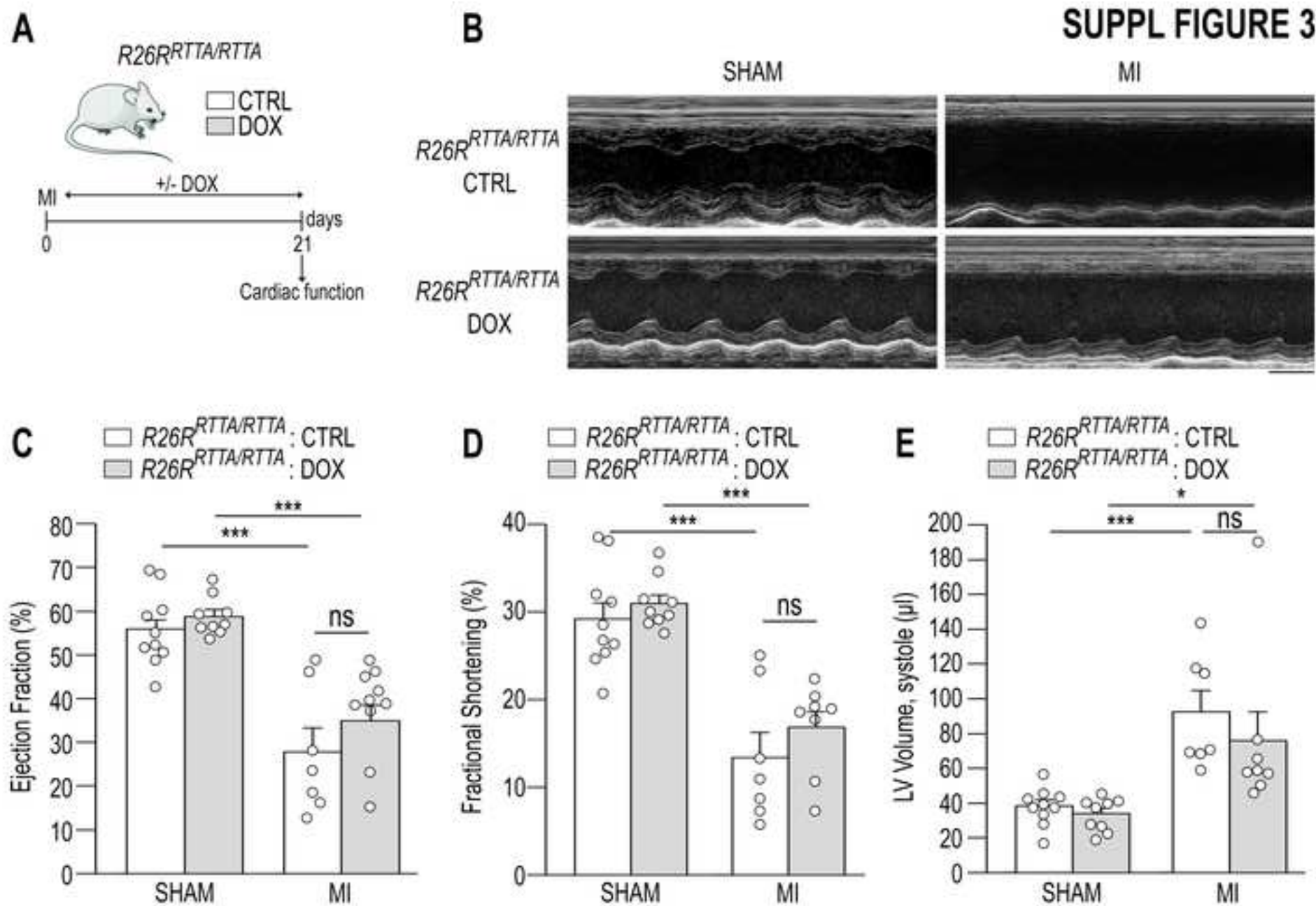
FIGURE 6



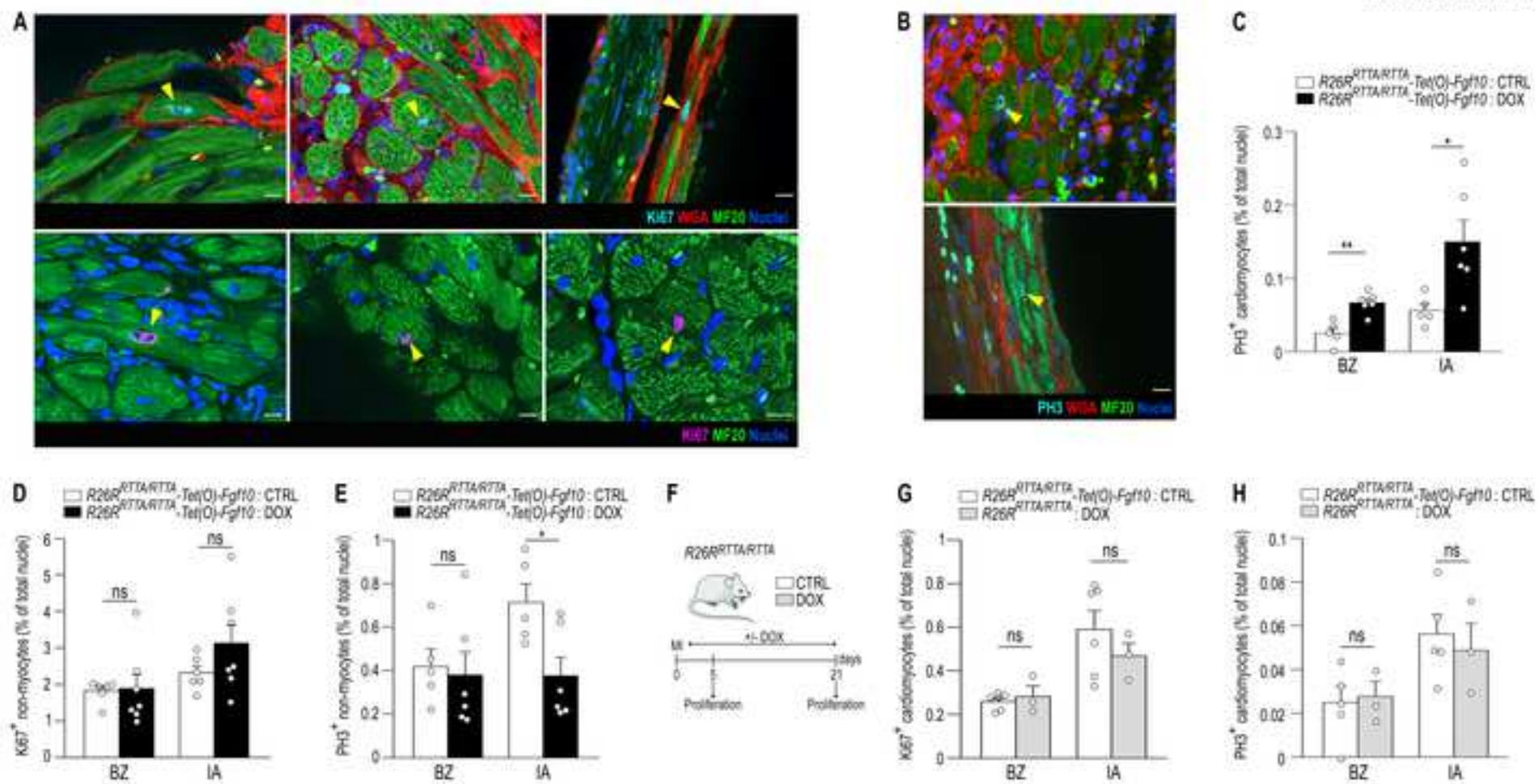


SUPPL FIGURE 2

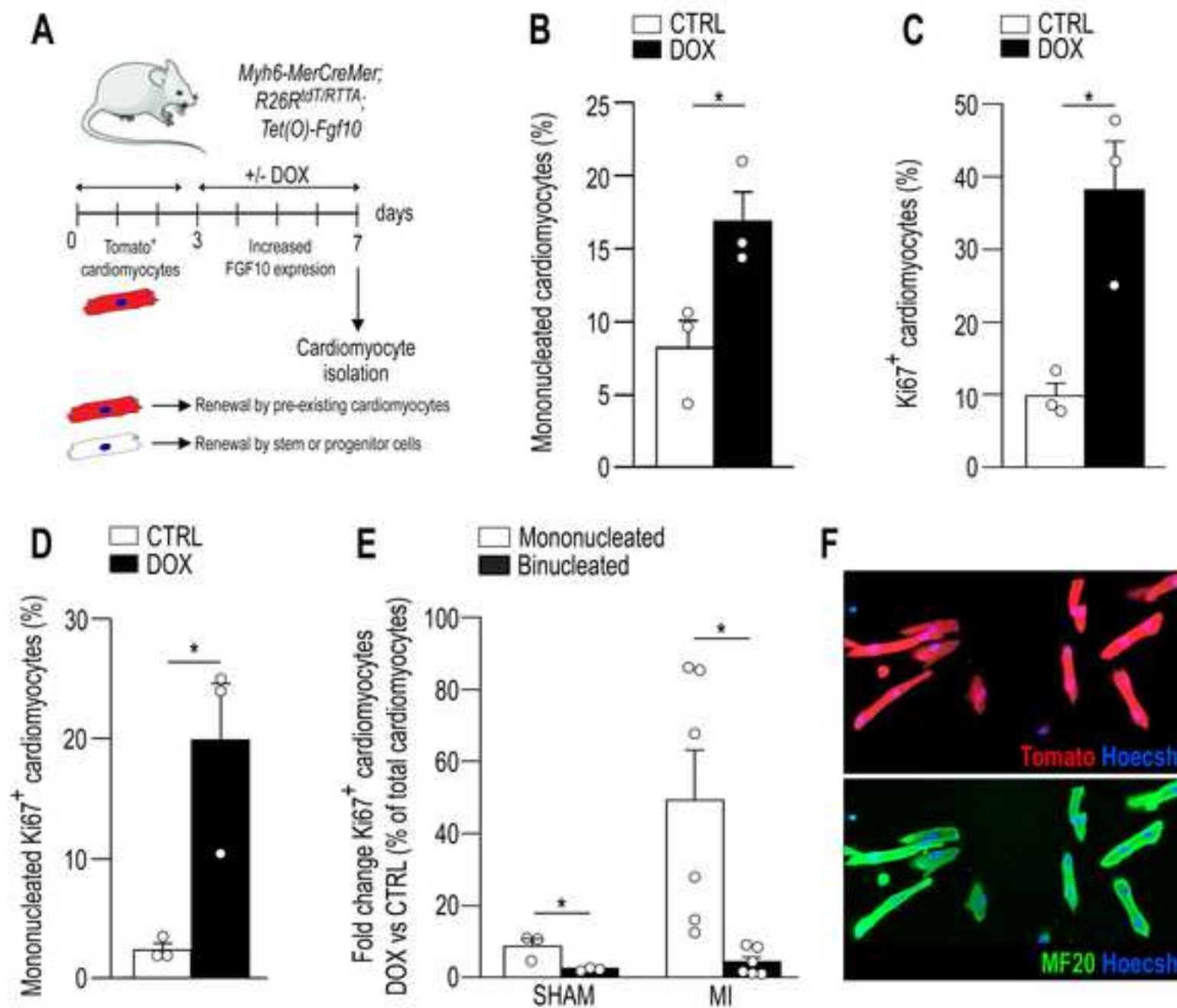


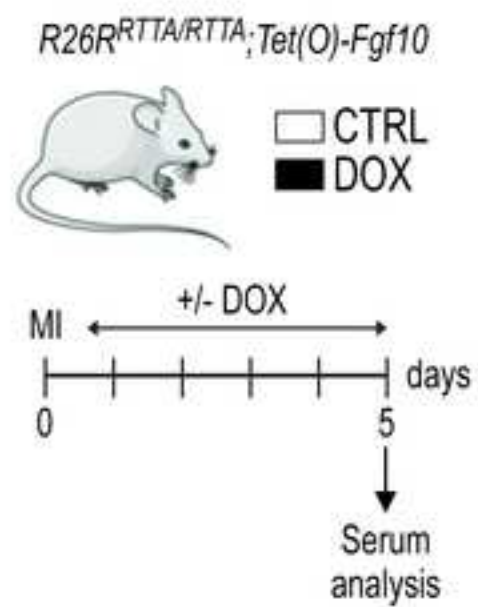
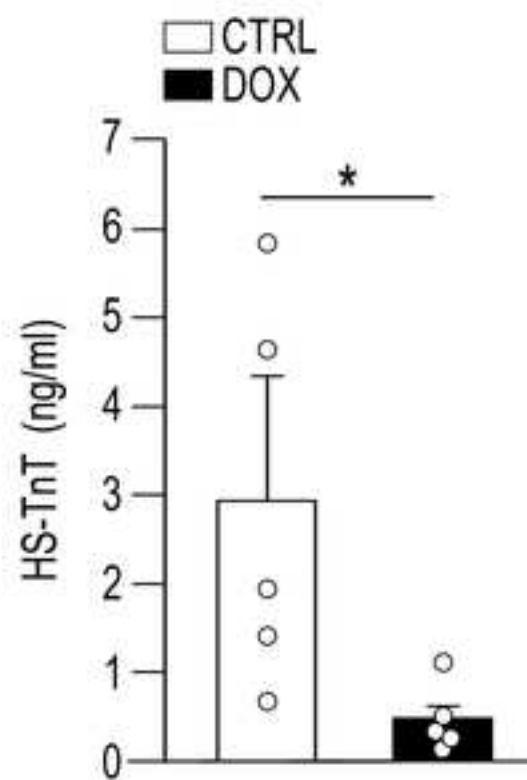
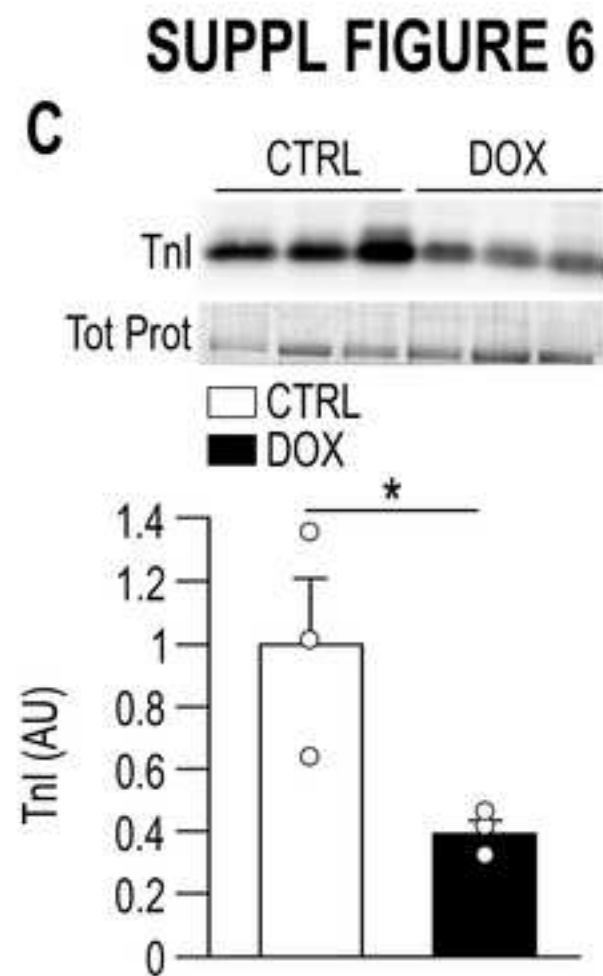


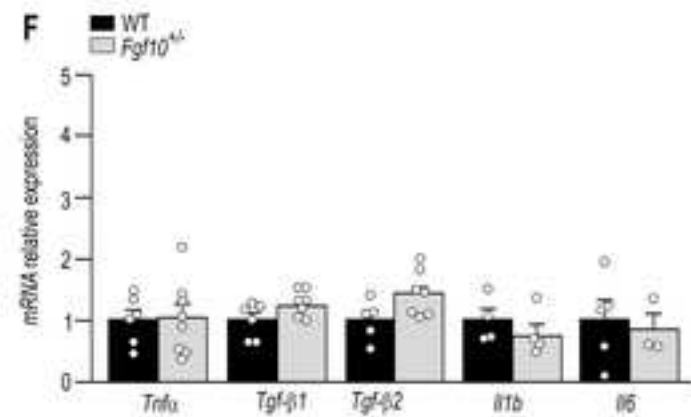
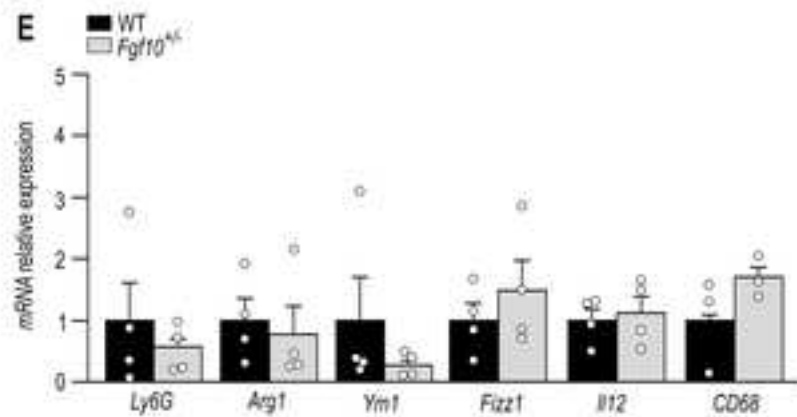
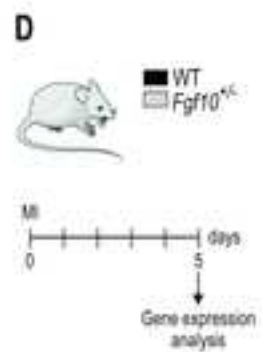
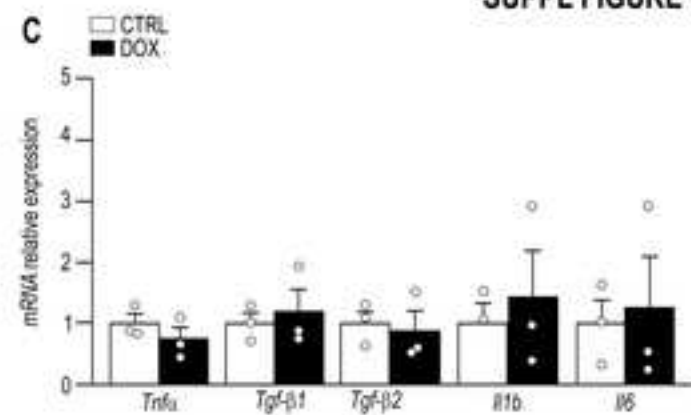
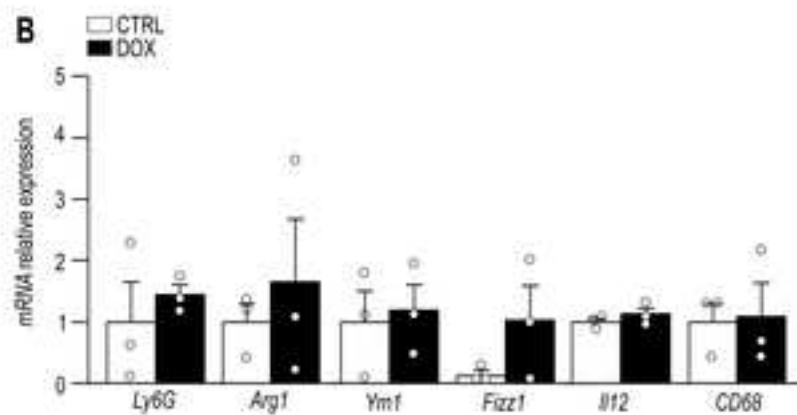
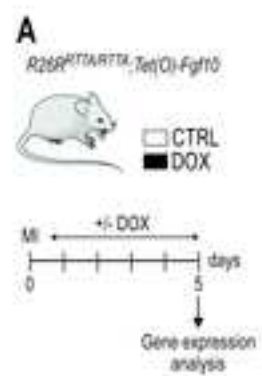
SUPPL FIGURE 4



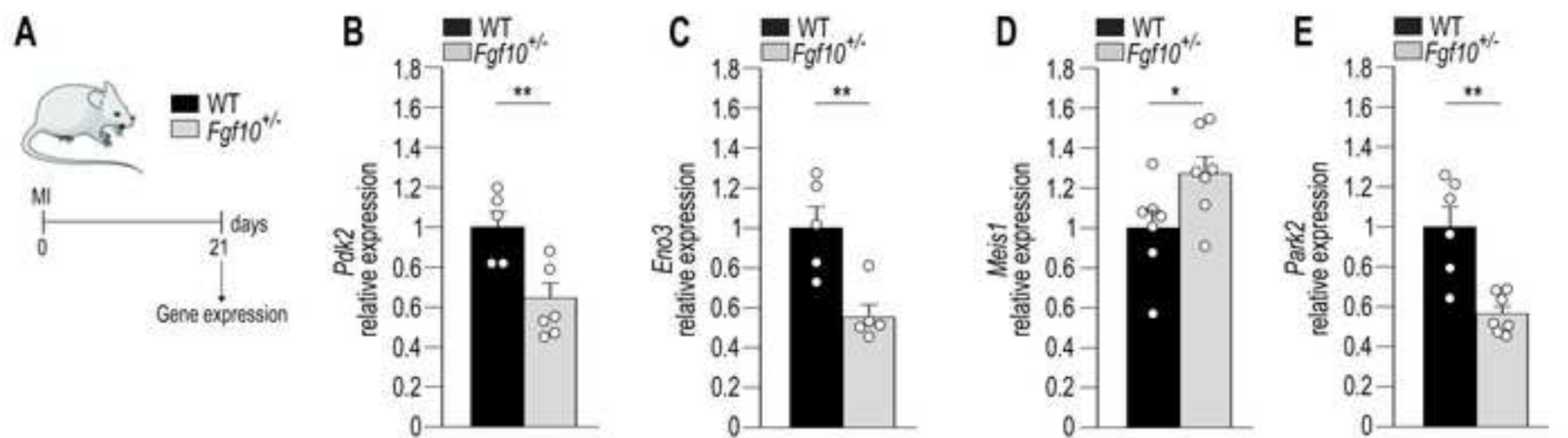
SUPPL FIGURE 5

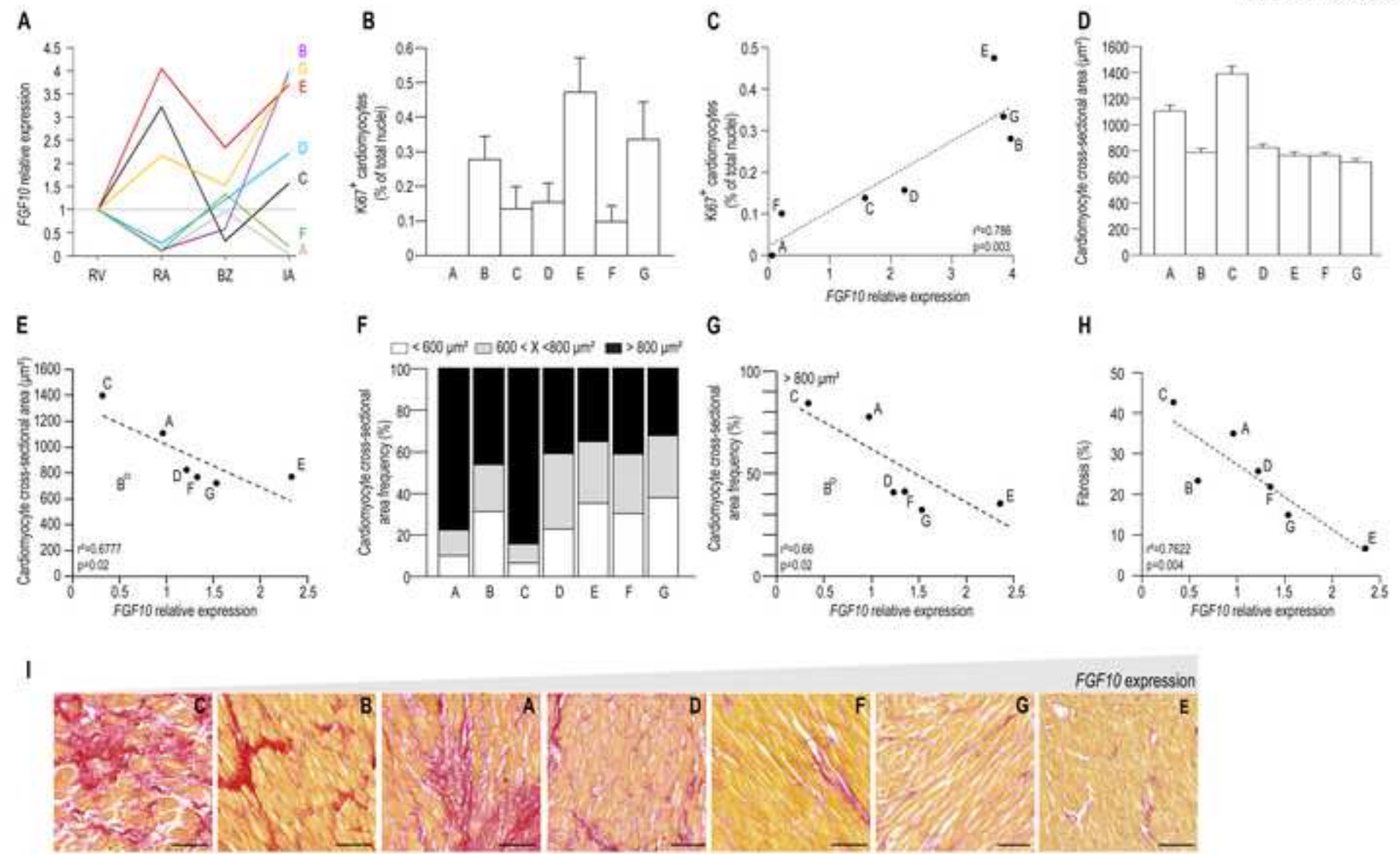


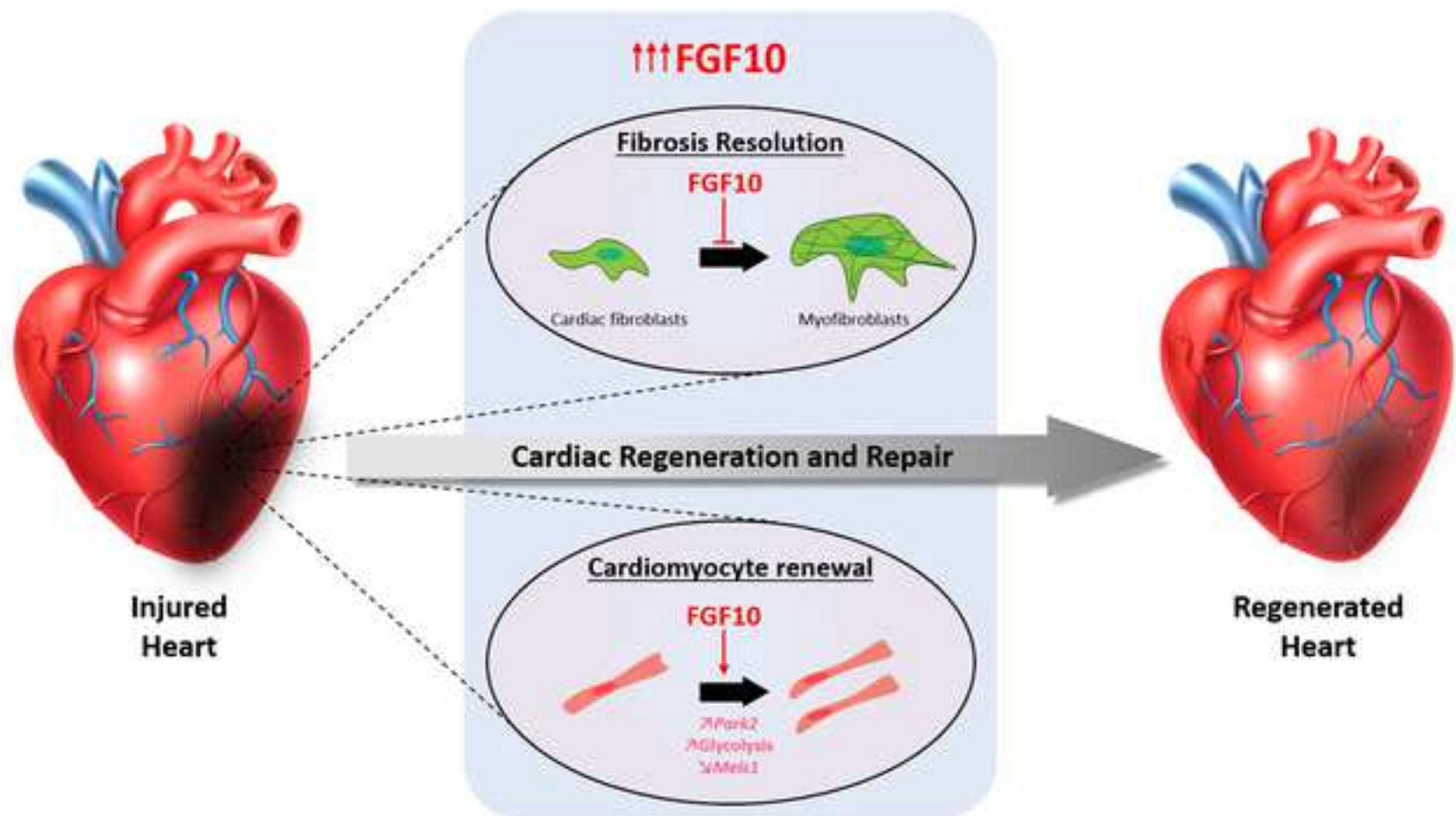
A**B****C**



SUPPL FIGURE 7







FGF10 promotes cardiac repair through a dual cellular mechanism increasing cardiomyocyte renewal and inhibiting fibrosis

Fabien Hubert PhD ^{1#}, Sandy M Payan PhD ^{1#}, Edeline Pelce MD-MSc ^{1,2}, Laetitia Bouchard MSc ¹, Rachel Sturny ³, Nicolas Lenfant PhD ¹, Giovanna Mottola PhD ^{4,5}, Frédéric Collart MD ², Robert G Kelly PhD ³ and Francesca Rochais PhD ¹

¹ Aix Marseille Univ, INSERM, MMG, U 1251, Marseille, France.

² Department of Cardiac Surgery, Timone Hospital, AP-HM, Marseille, France.

³ Aix Marseille Univ, CNRS UMR 7288, IBDM, Marseille, France.

⁴ Aix-Marseille Univ, C2VN, INSERM 1263, INRAE 1260, Marseille, France.

⁵ Laboratory of Biochemistry, Timone Hospital, Marseille, France.

These authors contributed equally

Address for correspondence

Dr. Francesca Rochais, Aix Marseille Université, MMG U1251

27 Boulevard Jean Moulin, 13005 Marseille, France

Phone : +334 91 32 48 86 ; FAX : +334 91 79 72 27

francesca.rochais@univ-amu.fr

ONLINE SUPPLEMENTAL METHODS

Mice. The genotyping PCR steps include pre-denaturation at 94°C for 5 minutes, 30 cycles of denaturation (94°C for 45 seconds), annealing (60°C for 45 seconds) and extension (72°C for 45 seconds) followed by a final extension step at 72°C for 7 minutes. PCR products were separated using agarose gel electrophoresis to detect the specific amplified fragments.

Primers for genotyping are listed in **Table 1**.

Mouse line	Primer	Sequence (5' - 3')
<i>Fgf10^{+/-}</i>	WT-FOR	CTCCAGTATGTTCTTCTGATGAGAC
	Mut-FOR	TACGGACAGTCTTCTTCTGGTCCC
	REV	GAGCTTGCTGGGGGAACTTCCTGACTAGG
<i>Fgf10-LacZ</i>	FOR	ATCCTCTGCATGGTCAGGTC
	REV	CGTGGCCTGATTCATTCC
<i>Rosa26-rtTA</i>	WT-FOR	AAGTCGCTCTGAGTTGTTATCAG
	WT-REV	GGAGCGGGAGAAATGGATATGA
	Mut-REV	CGGGTTGTAAACCTTCGATTCCG
<i>Tet(O)-Fgf10</i>	FOR	GACGCCATCCACGCTGT
	REV	TGCTGCCAGTTAAAAGATGC
<i>Rosa26-tdT</i>	WT-FOR	AAGGGAGCTGCAGTGGAGTA
	WT-REV	CCGAAAATCTGTGGGAAGTC
	Mut-FOR	CTGTTCTGTACGGCATGG
	Mut-REV	GGCATTAAAGCAGCGTATCC

<i>αMHC-</i>	FOR	AGGTTCGTTCACTCATGGA
<i>MerCreMer</i>	REV	TCGACCAGTTTAGTTACCC

Table 1: Genotyping PCR primer sequences.

Sirius red staining. Serial 13 μm sections were obtained and mounted on poly-lysine-treated slides. After dewaxing (xylene, 2 times) and rehydration in an ethanol series (100, 90, 70, 50% and H_2O), paraffin sections were incubated in a 0.1% Sirius Red solution dissolved in saturated aqueous solution of picric acid for 1 hour at room temperature. Subsequently, sections were washed 3 times in acidified water (0.5% acetic acid), dehydrated in ascending concentrations of ethanol (70%, 90% and 100%) and cleared in xylene. Sections were mounted in resinous medium (Entellan). Collagen and non-collagen components were red- and orange-stained, respectively.

Immunofluorescence. Serial 13 μm paraffin sections were obtained and mounted on slides. After dewaxing (xylene, 2 times) and rehydration in an ethanol series (100, 90, 70, 50% and H_2O), antigen was retrieved by boiling samples in Vector Antigen Unmasking Solution (Vector Laboratories, H-3300) for 15 min. Slides were allowed to cool to room temperature for 20 min and washed in PBS-Tween 0.05% (PBST). For blocking, samples were incubated for at least 1 hour in TNB (0.1M Tris-HCl, 0.15M NaCl, 0.5% (w/v)) blocking reagent (PerkinElmer FP1020) prior to incubation with antibodies in TNB overnight at 4°C. This was followed by 3 times PBS-T washes. Slides were then incubated with secondary antibody diluted in TNB for 1 hour at room temperature, followed by 3 washes in PBST and nuclei were counterstained with Hoescht (1/1000) and mounted using FluoroMount (Southern Biotech). Sections were imaged using a Zeiss AxioImager fluorescent microscope with an Apotome module.

Serial 13 μm cryostat sections were obtained from OCT embedded hearts. Sections were kept at room temperature for 15 min to dry and then washed with PBS. Slides were incubated for at least one hour in blocking solution (3% BSA-0.05% Saponin) prior to incubation with primary antibodies in blocking solution overnight at 4°C. This was followed by 3 washes in PBST. Slides were then incubated with secondary antibody in blocking solution for 1 hour at room temperature, followed by 3 washes in PBST. Nuclei were counterstained with Hoescht (1/1000) and mounted with FluoroMount (Southern Biotech). Sections were imaged using a Zeiss AxioImager fluorescent microscope with an Apotome module.

Cells attached onto coverslips were rinsed once in phosphate-buffered saline solution (PBS) for 5 min, fixed in paraformaldehyde 4% (5 min) and washed in PBS (3 times 5 min). The cells were then permeabilized in Triton X-100 0.5% (15 min), washed in PBS (2 times 5 min) and once in PBS-BSA 1% (5 min). Next, they were incubated 1 hour at 37°C with primary antibodies. After three washes in PBS and one in PBS-BSA 1%, the cells were revealed incubated with secondary antibodies (30 min, 37 °C). After three additional washes in PBS, nuclei were counterstained with Hoescht (1/1000) and the coverslips were mounted with FluoroMount (Southern Biotech) and then imaged using a Zeiss AxioImager fluorescent microscope with an Apotome module. Primary and secondary antibodies are listed in **Table 2**.

Primary antibodies			
α -actinin	Mouse	1/500	Sigma A7811
AURKB	Rabbit	1/400	Abcam ab2254
Caspase 3	Rabbit	1/100	Cell signalling 9665
β -galactosidase	Rabbit	1/500	MP Biomedicals 0855976
β -galactosidase	Chicken	1/1000	Abcam ab9361

Ki67	Rabbit	1/100	Abcam ab15580
MF20 sarcomeric myosin heavy chain	Mouse	1/50	DSHB
Phospho Histone H3	Rabbit	1/400	Upstate cell signalling 06-570
WGA-AlexaFluor555		1/50	Thermofisher W32464.
Secondary antibodies			
Anti-Rabbit Alexa Fluor 488	Donkey	1/500	ThermoFisher A-21206
Anti-Mouse Alexa Fluor 488	Donkey	1/500	ThermoFisher A-21202
Anti-Mouse Alexa Fluor 647	Donkey	1/500	ThermoFisher A-31571
Anti-Rabbit Alexa Fluor 647	Donkey	1/500	ThermoFisher A-21208

Table 2: Primary and secondary antibodies.

Quantitative Real Time PCR. Quantitative RT-PCR primers are listed in **Table 3.**

Gene	Species	Primer	Sequence (5' - 3')
<i>Acta2</i>	mouse	Acta2-F	ACTCTCTTCCAGCCATCTTTCA
	human	Acta2-R	ATAGGTGGTTTTCGTGGATGC
<i>Angpt1</i>	mouse	Angpt1-F	GGAAGATGGAAGCCTGGAT
		Angpt1-R	ACCAGAGGGATTCCCAAAC
<i>Ccnk</i>	mouse	Ccnk-F	GTTTGGAGATGACCCAAAGG
		Ccnk-R	AAGTCAAACCTTTATGGTCTGCAGTAA
<i>Cdkn2b</i>	mouse	Cdkn2b-F	AATAACTTCTACGCATTTTCTGC
		Cdkn2b-R	CCCTTGGCTTCAAGGTGAG
<i>Col1A1</i>	mouse	Col1A1-F	CATGTTTCAGCTTTGTGGACCT

		Col1A1-R	GCAGCTGACTTCAGGGATGT
<i>Col3A1</i>	mouse	Col3A1-F	TGGTCCTGCTGGAAAGGAT
		Col3A1-R	GAGGTCCAGGCAGTCCAC
<i>Col6A5</i>	mouse	Col6A5-F	CCTCCTGGTCGGAGAGGT
		Col6A5-R	TTCACAGGGGGAATATATAGGTTG
<i>Crispld2</i>	mouse	Crispld2-F	AGGTTGAGGCCAGAGTTCC
		Crispld2-R	GCCTTCAGCCACA ACTAAGAG
<i>Ddr2</i>	mouse	Ddr2-F	ATGTTGGCAGGCAAGACAG
		Ddr2-R	TCAGGTCGCTGTAGATTTCC
<i>Efnb3</i>	mouse	Efnb3-F	TGGA ACTCGGCGAATAAGAG
		Efnb3-R	CCCCGATCTGAGGATAAAGC
<i>Eno3</i>	mouse	Eno3-F	ACACAGCCAAGGGTCGATT
		Eno3-R	TCCACAGCCTTCAGCACTC
<i>ErbB3</i>	mouse	ErbB3-F	CACGAGA ACTGCACCCAAG
		ErbB3-R	TCTGCTTGGCCTAAACAGTCT
<i>Fgf10</i>	mouse	Fgf10-F	GAGAAGAACGGCAAGGTCAG
	rat	Fgf10-R	TTTCCCCTTCTTGTTTCATGG
	human	FGF10-F	GAAGGAGA ACTGCCCGTACA
		FGF10-R	GGCAACA ACTCCGATTTCTACT
<i>Hprt</i>	mouse	Hprt-F	CTGGTGAAAAGGACCTCTCG
		Hprt-R	TGGCAACATCAACAGGACTC
<i>Homer2</i>	mouse	Homer2-F	CCAGAGACAAGTCCCAGGAG
		Homer2-R	CCATTGACGCTGGATGCT

<i>IL-1b</i>	mouse	IL-1b-F	AGTTGACGGACCCCAAAG
		IL-1b-R	TTTGAAGCTGGATGCTCTCAT
<i>IL-6</i>	mouse	IL-6 F	GATGGATGCTACCAAAGTGGAT
		IL-6 R	CCAGGTAGCTATGGTACTCCAGA
<i>Isl1</i>	mouse	Isl1-F	AGCAACCCAACGACAAAAGT
		Isl1-R	CCATCATGTCTCTCCGGACT
<i>Mdh1</i>	mouse	Mdh1-F	TGCTCTACTCATTCCCTGTCTG
		Mdh1-R	CCTTTGCTGTCAGGTCCATC
<i>Meis1</i>	mouse	Meis1-F	ATGGGTTCCCTCGGTCAATG
		Meis1-R	CATTTCTCAAAAATCAGTGCTAAGA
<i>Myh6</i>	mouse	Myh6-F	CCTCAAGCTCATGGCTACAC
		Myh6-R	TTGCCTCCTTTGCCTTTACC
<i>Myh7</i>	mouse	Myh7-F	AGGCAAAGAAAGGCTCATCC
		Myh7-R	TGGAGCGCAAGTTTGTGATA
<i>Nkx2.5</i>	mouse	Nkx2.5-F	CAAGTGCTCTCCTGCTTTCC
		Nkx2.5-R	CTTTGTCCAGCTCCACTGC
<i>Nppa</i>	mouse	Nppa -F	CAACACAGATCTGATGGATTTCA
		Nppa -R	CCTCATCTTCTACCGGCATC
<i>Nppb</i>	mouse	Nppb -F	GTCAGTCGTTTGGGCTGTAAC
		Nppb -R	AGACCCAGGCAGAGTCAGAA
<i>Park2</i>	mouse	Park2-F	CGCGTAGGTCCTTCTCGAC
		Park2-R	GAAAGGCTGGGCCTAGATACA
<i>Pdgfra</i>	mouse	Pdgfra-F	AAGACCTGGGCAAGAGGAAC

		Pdgfra-R	GAACCTGTCTCGATGGCACT
<i>Pdha1</i>	mouse	Pdha1-F	GTAAGGGGCCCATCCTGA
		Pdha1-R	TCTTCTCGAGTGCGGTAGC
<i>Pdhb</i>	mouse	Pdhb-F	TGATGAAGACAAATCATCTCGTG
		Pdhb-R	AGGGGCATCAAGGAAGTTG
<i>Pdk1</i>	rat	Pdk1-F	CCGATTCAAGTTCACGTCAC
		Pdk1-R	ACCTCCCCGGTCACTCAT
<i>Pdk2</i>	mouse	Pdk2-F	TGGCTAAGCTCCTGTGTGAC
		Pdk2-R	CATGTGAATGGGCTGGTTG
<i>Pecam1</i>	mouse	CD31-F	CGGTGTTCAGCGAGATCC
		CD31-R	ACTCGACAGGATGGAAATCA
<i>Pfkm</i>	mouse	Pfkm-F	GGACAATCTGCAAGAAAGCA
		Pfkm-R	TGATGCTCTTCATGGGTCAT
<i>pfkp</i>	mouse	Pfkp-F	GAGGGACCCCATCTGCAT
		Pfkp-R	GTAGCTTCCAGCAAGGCAAT
<i>Ppargc1a</i>	mouse	Ppargc1a-F	AGCCTGCGAACATATTTGAGA
		Ppargc1a-R	ATGAGGGCAATCCGTCTTC
<i>PPIA</i>	Human	PPIA-F	ATGCTGGACCCAACACAAAT
		PPIA-R	TCTTTCACCTTTGCCAAACACC
<i>Prkaa2</i>	mouse	Prkaa2-F	CGACTACATCTGCAAACATGG
		Prkaa2-R	CAGTAATCCACGGCAGACAG
<i>Smoc1</i>	mouse	Smoc1-F	GATAAGGTCATCTCACTGCCTGA
		Smoc1-R	AAGCTGCCAAGGCTACCAC

<i>Smoc2</i>	mouse	Smoc2-F	CGTGGAATTGCAAAGATG
		Smoc2-R	CCTGCTCCTGGGTATACTTCC
<i>Tbx1</i>	mouse	Tbx1-F	TTTGTGCCCCTAGATGACAA
		Tbx1-R	ACTCGGCCAGGTGTAGCA
<i>Tcf7</i>	mouse	Tcf7-F	AGGAGCTGCAGCCATATGAT
		Tcf7-R	TGACTGGCTTCTTAGCCTCCT
<i>TGFb1</i>	mouse	TGFb1-F	TGGAGCAACATGTGGAAGCTC
		TGFb1-R	GTCAGCAGCCGGTTACCA
<i>TGFb2</i>	mouse	TGFb2-F	AGGAGGTTTATAAAATCGACATGC
		TGFb2-R	TAGAAAGTGGGCGGGATG
<i>TGFb3</i>	mouse	TGFb3-F	CCCTGGACACCAATTACTGC
		TGFb3-R	TCAATATAAAGGGGGCGTACA
<i>Tnfα</i>	mouse	TNF α -F	AGCCTCTTCTCATTCTGCTT
		TNF α -R	ATGAGAGGGAGGCCATTTG.
<i>Vegfb</i>	mouse	Vegfb-F	GCTCAACCCAGACACCTGTAG
		Vegfb-R	AGGAGGTTTCGCCTGTGCT
<i>Vegfc</i>	mouse	Vegfc-F	GAGTCGGGACTGGGCTTC
		Vegfc-R	GACACAGACCGCAACTGCT
YWHAZ	human	YWHAZ-F	GTGGACATCGGATACCCAAG
		YWHAZ-R	AAGTTGGAAGGCCGGTTAAT

Table 3: Quantitative RT-PCR primer sequences.

Data processing and differential gene expression (DGE) analysis.

70 millions of reads (clusters) have been sequenced, on average, by sample. The quality of sequencing reads was assessed using fastQC¹. Reads were mapped to the mouse reference genome (GRCm38/mm10) using STAR (v2.5.3a)² and bam files were indexed and sorted using Sambamba (v0.6.6)³. Number of read fragments per gene (GENCODE annotations) was determined after mapping using Stringtie (v1.3.1c)⁴. Differential gene expression analysis was performed using DESeq2⁵. p-values were adjusted for multiple testing using the method by Benjamini and Hochberg⁶ and genes with an FDR (False Discovery Rate) adjusted p-value below 0.05 were considered as significantly differentially expressed. The heatmap of Differentially Expressed Genes using was generated using the Pheatmap R package, while the volcano plot representing the Log₂FC (log₂ of the expression fold change) and the adjusted p-value of the Wald test has been prepared by using the EnhancedVolcano R package. Enrichment (Gene set enrichment Analysis, GSEA) and overrepresentation (Singular Enrichment Analysis, SEA) in GO term analysis were performed using a Mann-Whitney test and hypergeometric test respectively, thanks to the ClusterProfiler R package. In the case of over-representation, the test was set on genes having a FDR adjusted p-value below 0.001, the value commonly accepted as threshold for significance. Results of GSEA and SEA, have been represented, for a set of selected genes, as Circos plot with GOplot R package.

¹Andrews S. Fastqc: A Quality Control Tool for High Throughput Sequence Data. Available online at <https://www.bioinformatics.babraham.ac.uk/projects/fastqc>. 2010.

²Dobin A and Gingeras TR. Mapping RNA-seq Reads with STAR. Current Protocols in Bioinformatics. 2015; 51(1), 11.14.1-11.14.19.

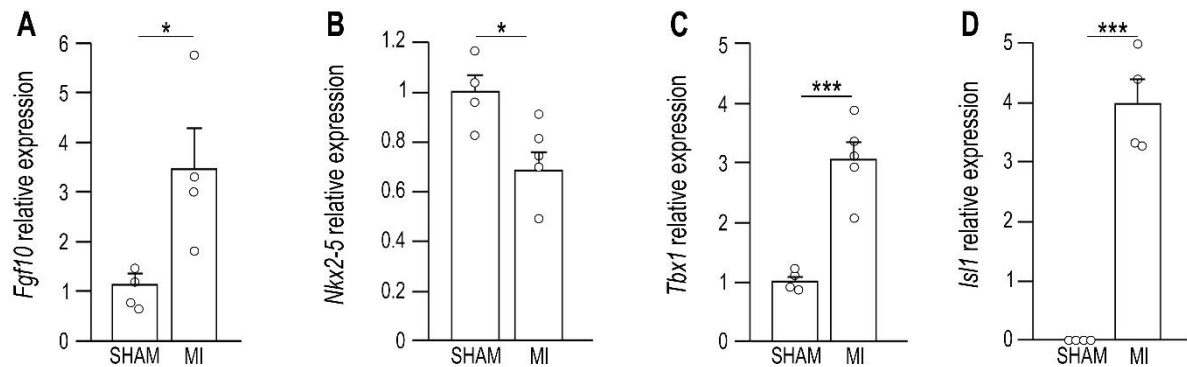
³Tarasov A, Vilella AJ, Cuppen E, Nijman IJ and Prins P. Sambamba: fast processing of NGS alignment formats. *Bioinformatics*. 2015; 31(12): 2032–2034.

⁴Pertea M, Pertea GM, Antonescu CM, Chang TC, Mendell JT and Salzberg SL. StringTie enables improved reconstruction of a transcriptome from RNA-seq reads. *Nature Biotechnology*. 2015; 33(3), 290–295.

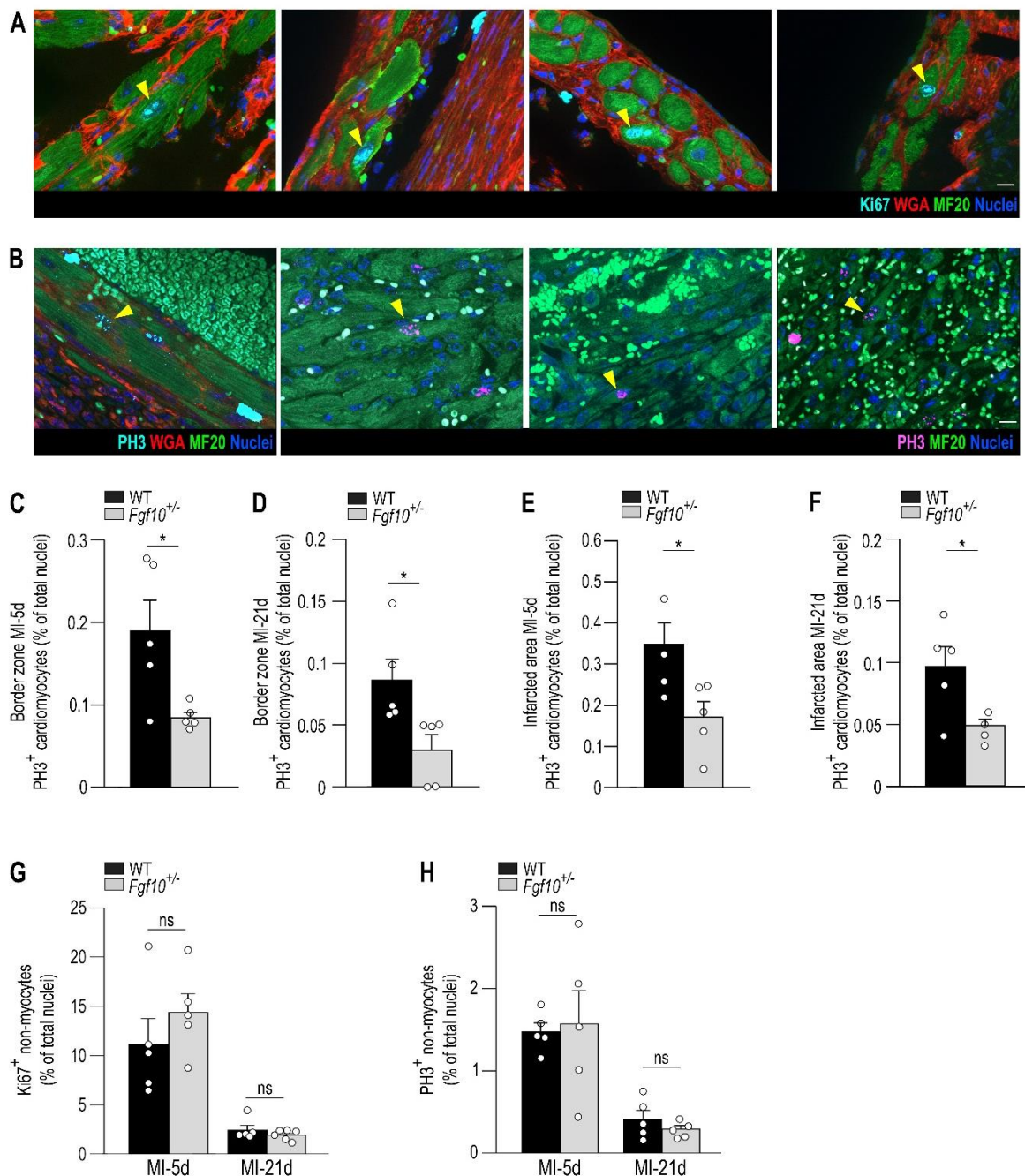
⁵Love MI, Huber W and Anders S. Moderated estimation of fold change and dispersion for RNA-seq data with DESeq2. *Genome Biol*. 2014; 15(12): 550.

⁶Benjamini Y and Hochberg Y. Controlling the false discovery rate: a practical and powerful approach to multiple testing. *J R Stat Soc B*. 1995; 57, 289-300.

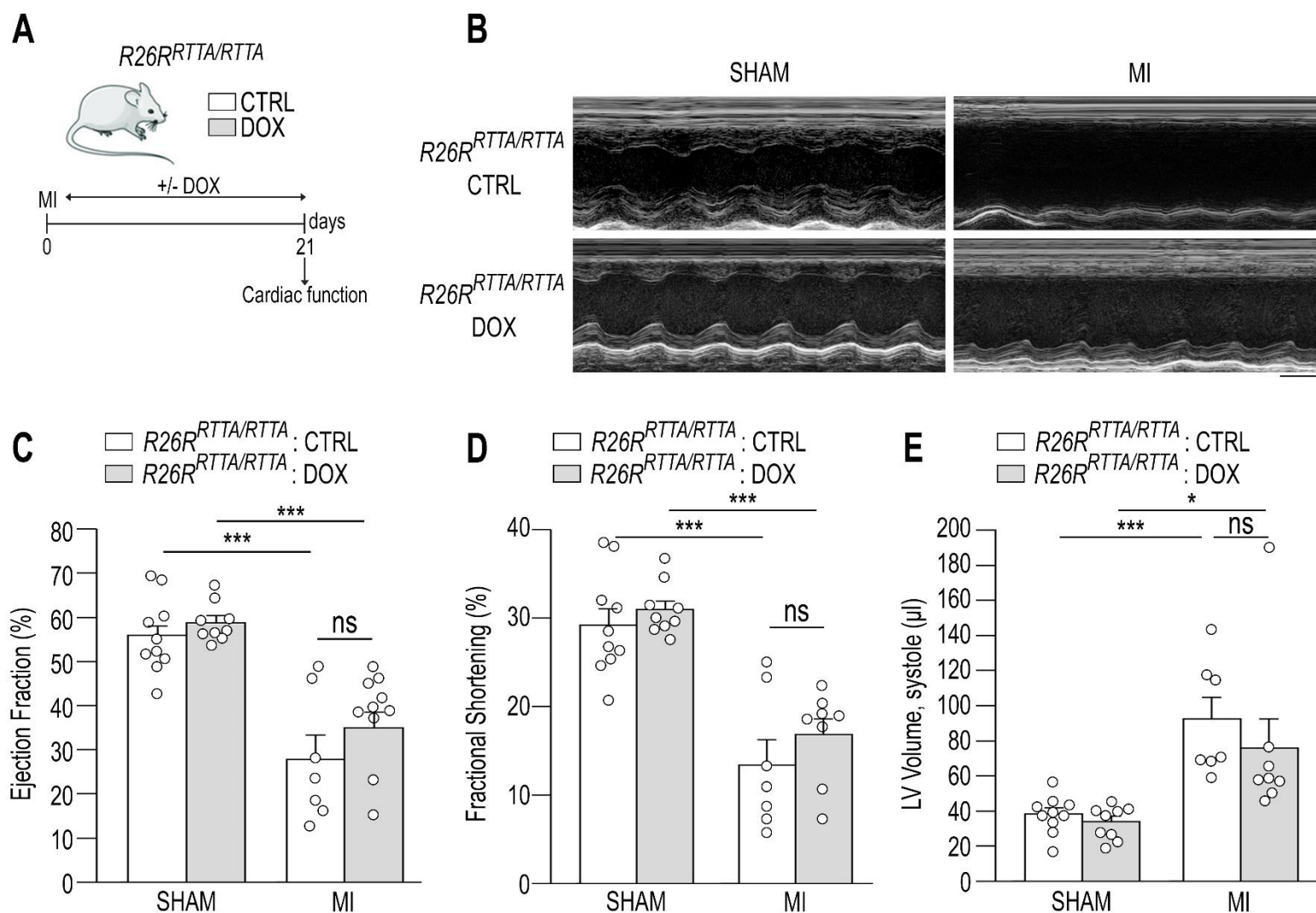
ONLINE SUPPLEMENTAL FIGURES



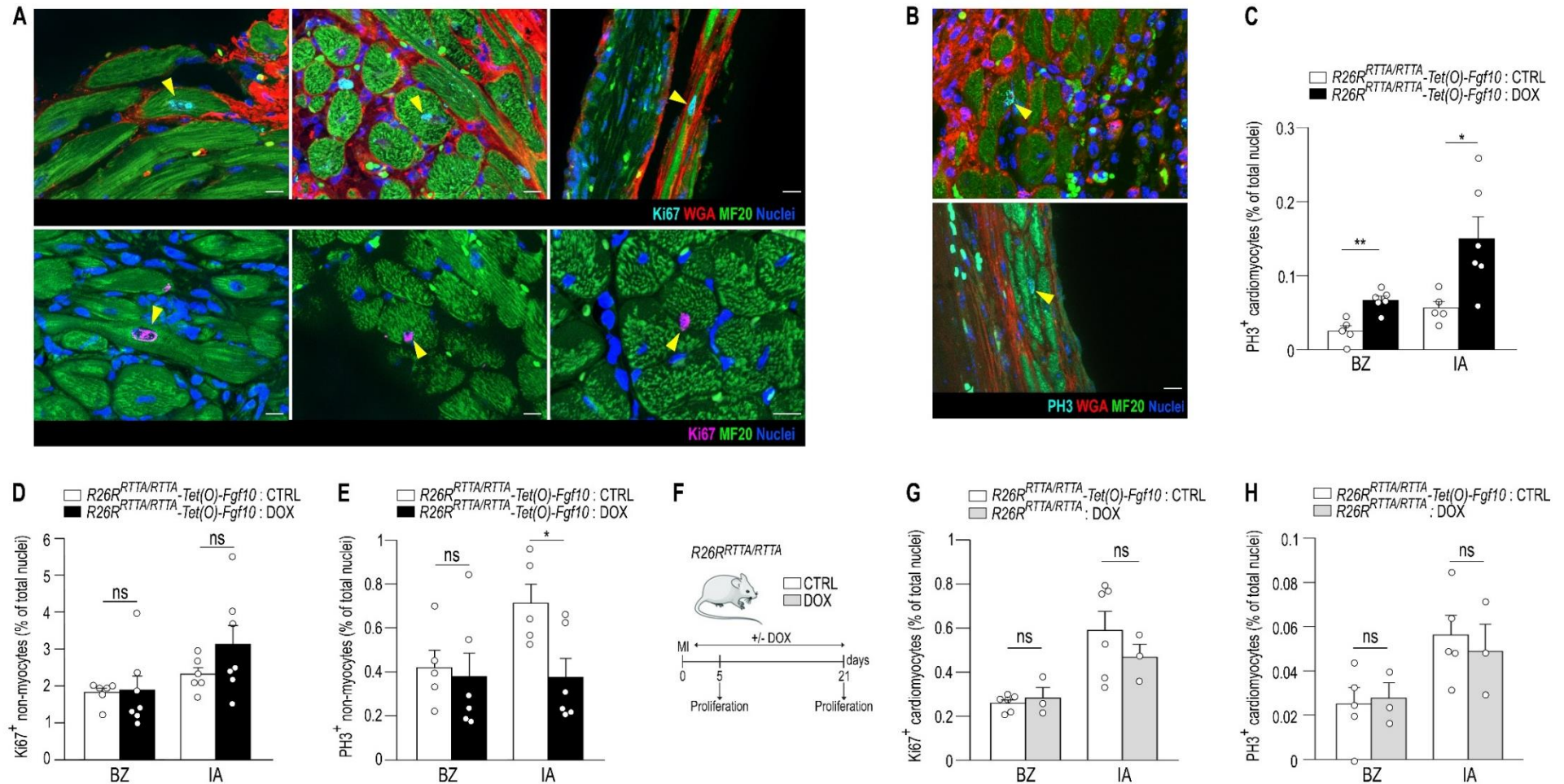
Supplemental Figure 1: *Fgf10* expression is upregulated after myocardial infarction (MI). qRT-PCR experiments on left ventricular MI hearts showing (A) *Fgf10*, (B) *Nkx2-5*, (C) *Tbx1* and (D) *Isl1* expression 21 days after MI (n=4-5 per group). *Isl1* expression is normalized to right ventricular expression. *, p<0.05; ***, p<0.001; Student's t-test.



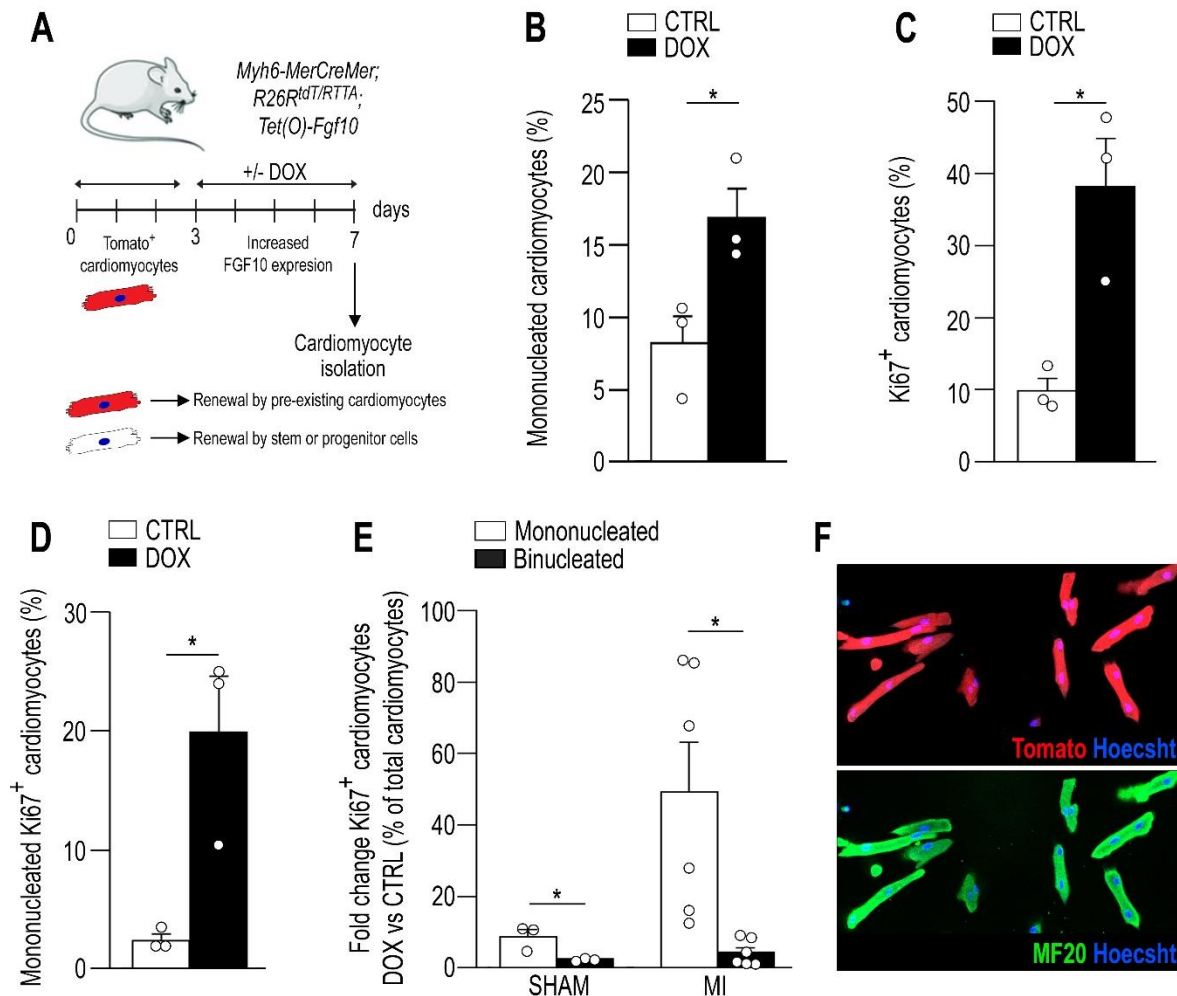
Supplemental Figure 2: Decreased *Fgf10* dosage impairs maximal cardiomyocyte proliferation post-MI. WT and *Fgf10*^{+/-} adult mice were subjected to myocardial infarction. Immunofluorescence experiments on paraffin sections were performed to evaluate, in the border zone, *in vivo* cardiomyocyte proliferation (MF20⁺; yellow arrowheads) post-MI using Ki67 (A) and PH3 (B). Border zone *in vivo* cardiomyocyte proliferation (PH3⁺MF20⁺; yellow arrowheads) 5 days (C; n=5/group) and 21 days (D; n=5/group) post-MI. Infarcted area *in vivo* cardiomyocyte proliferation (PH3⁺MF20⁺; yellow arrowheads) 5 days (E; MI-5d; n=5/group) and 21 days (F; MI-21d; n=5/group) post-MI. *In vivo* non-myocyte proliferation (MF20⁻), in the border zone, was determined 5 (WT, n=5; *Fgf10*^{+/-}, n=5) and 21 (WT, n=5; *Fgf10*^{+/-}, n=6) days post-MI using Ki67 (G) and PH3 (H). Scale bars 10 μ m. ns, non-significant; *, p < 0.05; Student's t-test.



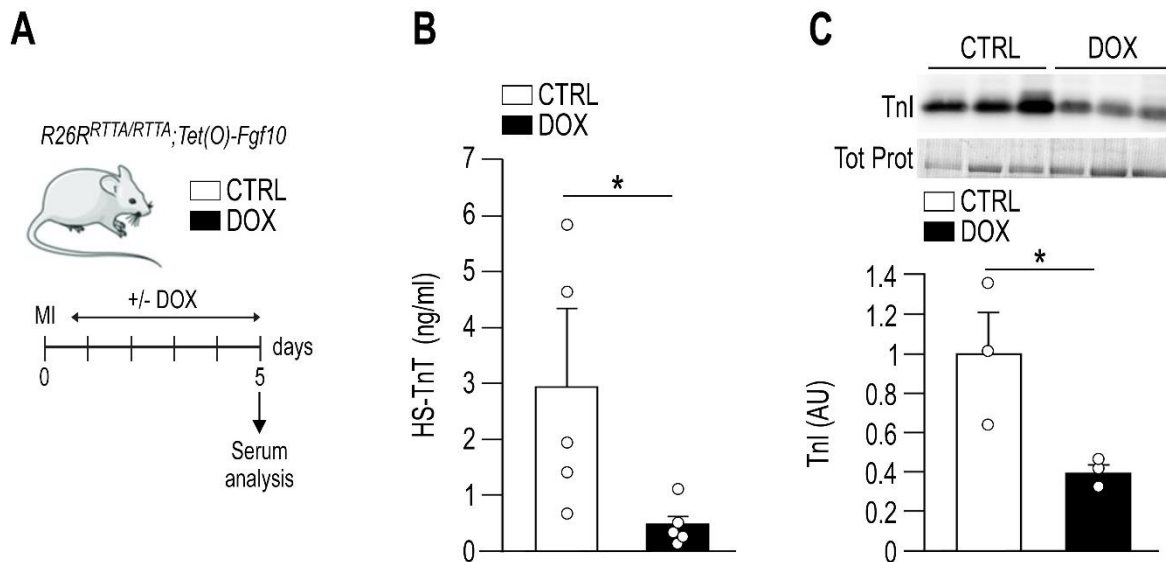
Supplemental Figure 3: Upregulation of *Fgf10* levels post-MI preserves cardiac function and remodeling. (A) Schematic of the experimental plan. *R26R-RTTA* mice were subjected to myocardial infarction (MI). One day after MI, mice were fed with normal (CTRL) or doxycycline supplemented food (DOX). (B) M-mode images of echocardiographic experiments (Scale bars, x: 0.1 s; y: 1 mm). (C) Ejection fraction, (D) fractional shortening and (E) left ventricular systolic volume. SHAM-CTRL, n=10; SHAM-DOX, n=9; MI-CTRL, n=7; MI-DOX, n=8. ns, non-significant; *, p<0.05; ***, p<0.001; Student's *t*-test.



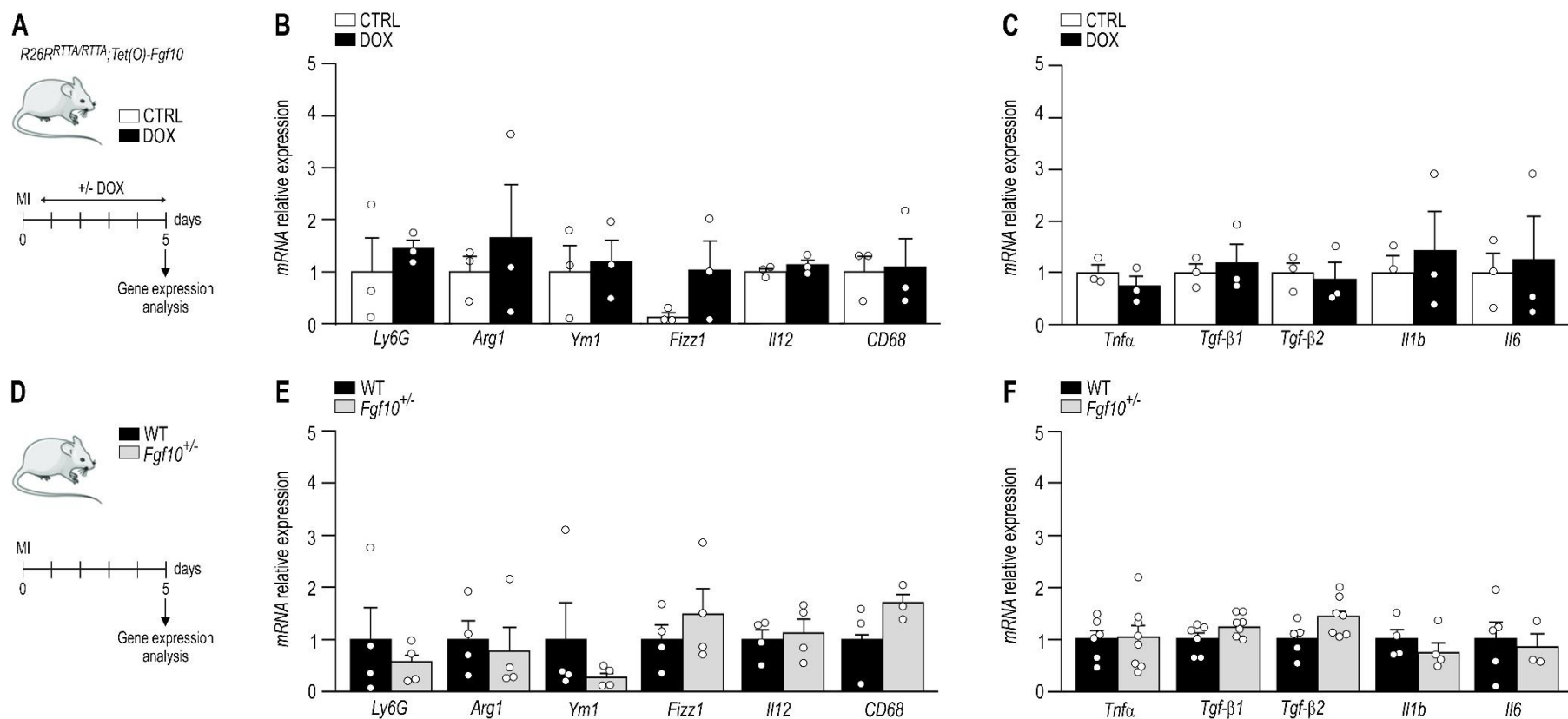
Supplemental Figure 4: Upregulation of *Fgf10* levels post-MI promotes cardiomyocyte cell cycle reentry. (A-E) *R26R-RTTA/Tet(O)-Fgf10* mice were subjected to myocardial infarction (MI). One day after MI, mice were fed with normal (CTRL) or doxycycline (DOX) supplemented food. Immunofluorescence experiments on paraffin sections were performed 21 days post-MI to evaluate cell proliferation in the border zone (BZ) and in the infarcted area (IA). Cardiomyocyte proliferation was detected using Ki67 (A) and PH3 markers (B-C; *R26R-RTTA/Tet(O)-Fgf10*:CTRL n=5; *R26R-RTTA/Tet(O)-Fgf10*:DOX n=6). Scale bars: 10 μ m. (D-E) Non-myocyte proliferation was detected by Ki67⁺ (D; *R26R-RTTA/Tet(O)-Fgf10*:CTRL n=6; *R26R-RTTA/Tet(O)-Fgf10*:DOX n=7) and PH3 (E, *R26R-RTTA/Tet(O)-Fgf10*:CTRL n=5; *R26R-RTTA/Tet(O)-Fgf10*:DOX n=6) markers. (F-H) *R26R-RTTA* mice were subjected to myocardial infarction (MI). One day after MI, mice were fed with normal (CTRL) or doxycycline (DOX) supplemented food. Immunofluorescence experiments on paraffin sections were performed, 21 days post-MI, to evaluate cell proliferation in the border zone (BZ) and in the infarcted area (IA; *R26R-RTTA/Tet(O)-Fgf10*:CTRL n=6, *R26R-RTTA*:DOX n=3). ns, non-significant; *, p < 0.05; **, 0.001 < p < 0.01; Student's *t*-test.



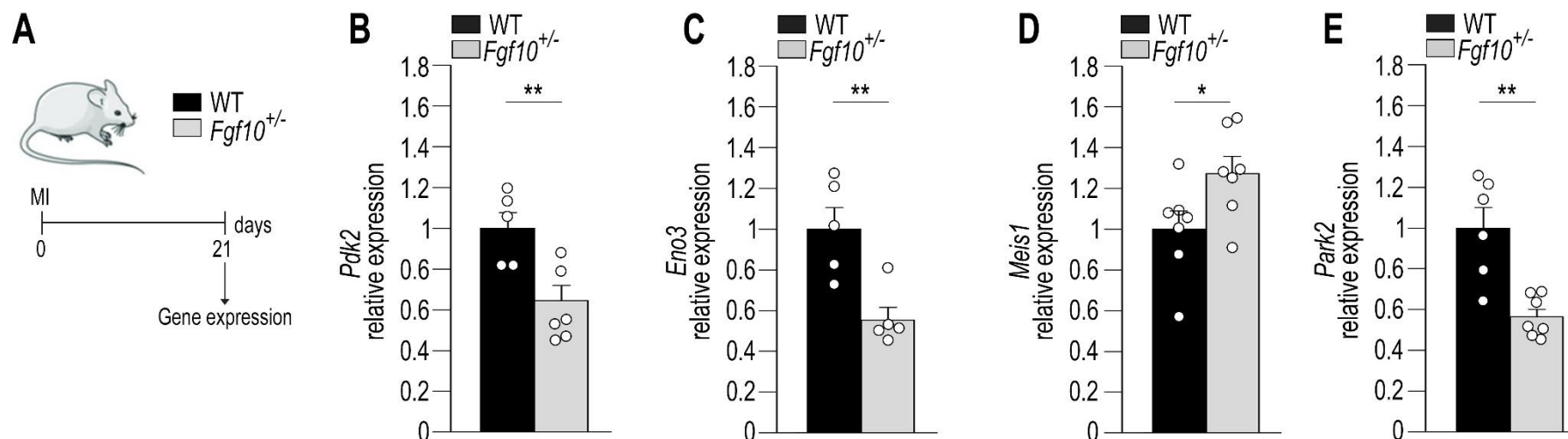
Supplemental Figure 5: Upregulation of *Fgf10* levels promotes cardiomyocyte renewal. (A) α MHC-MerCreMer/R26R-tdT/R26R-RTTA/Tet(O)-*Fgf10* mice were injected with Tamoxifen (Tam) and then fed with doxycycline (DOX) supplemented food for 5 days. (B-D) Cardiomyocytes were isolated and immunofluorescence experiments were performed to evaluate mononucleated cardiomyocyte proliferative capacities. (E) Cardiomyocytes were isolated and immunofluorescence experiments were performed to evaluate mono- and binucleated cardiomyocyte proliferative capacities in normal (SHAM; n=3) and myocardial infarction (MI; n=6) conditions. (F) Cardiomyocytes were isolated and immunofluorescence experiments were performed to evaluate cardiomyocyte lineage.



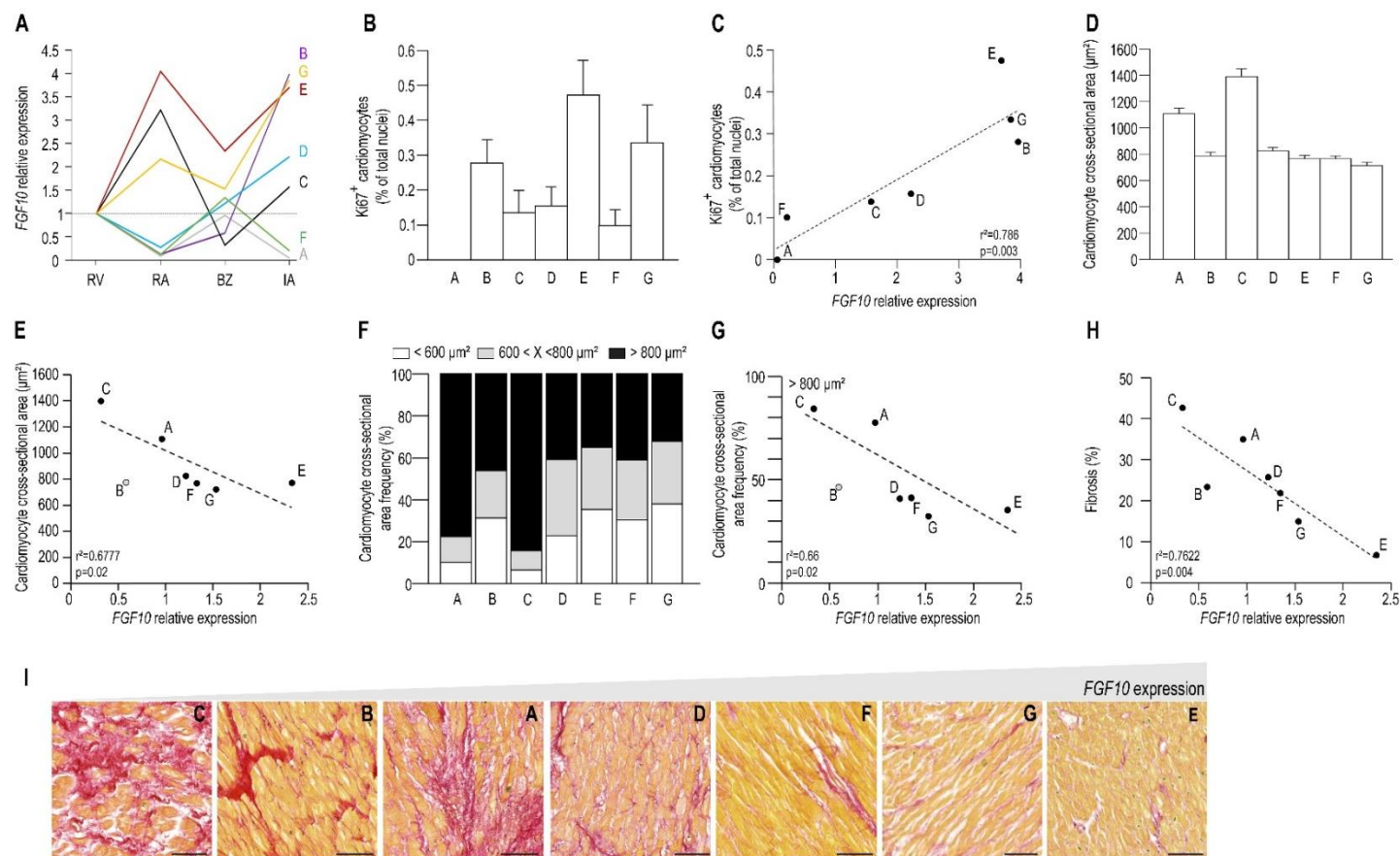
Supplemental Figure 6: Upregulation of *Fgf10* levels post-MI prevents cardiomyocyte cell death. (A) *R26R-RTTA/Tet(O)-Fgf10* mice were subjected to myocardial infarction (MI). One day after MI, mice were fed with normal (CTRL) or doxycycline (DOX) supplemented food for 5 days. (B) High-sensitive cardiac troponin T (HS-TnT) serum level analysis (n=5 per group). (C) Western blot experiment revealing reduced cardiac Troponin I (TnI) serum levels in DOX- compared to CTRL-treated animals post-MI (n=3 per group). *, p<0.05; Student's *t*-test.



Supplemental Figure 7: Impact of modulated *Fgf10* expression on myocardial inflammation post-MI. (A-C) *R26R-RTTA/Tet(O)-Fgf10* mice were subjected to myocardial infarction (MI). One day after MI, mice were fed with normal (CTRL) or doxycycline (DOX) supplemented food for 5 days. qRT-PCR analysis of key inflammatory cell (B) and cytokine (C) gene expression in the infarcted area 5 days post-MI. n=3-8 per group. (D-F) WT and *Fgf10*^{+/-} adult mice were subjected to myocardial infarction. qRT-PCR analysis of key inflammatory cell (E) and cytokine (F) gene expression in the infarcted area 5 days post-MI. n=3-8 per group.



Supplemental Figure 8: Impact of decreased *Fgf10* dosage on *Pdk2*, *Eno3*, *Meis1* and *Park2* expression following MI. (A) Schematic of the experimental plan. WT and *Fgf10*^{+/-} adult mice were subjected to myocardial infarction (MI) and analysis were performed 21 days after surgery. qRT-PCR analysis 21 days post-MI of (B) *Pdk2* (WT, n=5; *Fgf10*^{+/-}, n=6), (C) *Eno3* (WT, n=5; *Fgf10*^{+/-}, n=5), (D) *Meis1* (WT, n=7; *Fgf10*^{+/-}, n=7) and (E) *Park2* (WT, n=6; *Fgf10*^{+/-}, n=7) expression in the infarcted area. ns, non-significant; *, p<0.05; **, 0,001<p<0.01; Student's *t*-test.



Supplemental Figure 9: *FGF10* upregulated levels in human failing heart correlate with increased cardiomyocyte proliferation, reduced cardiomyocyte size and reduced fibrosis. Human explanted failing heart samples from right ventricle (RV), remote area (RA), border zone (BZ) and infarcted area (IA) were collected from 7 patients (A-G). (A) qRT-PCR experiments revealed upregulated *FGF10* levels in the BZ (4 patients out of 7) and the IA (5 patients out of 7). (B) Cardiomyocyte proliferation in the infarcted area was evaluated using immunofluorescence experiments on paraffin sections and the cell cycle marker Ki67. (C) Elevated *FGF10* levels correlate with enhanced cardiomyocyte proliferation in the IA ($r^2=0.786$, $p=0.003$). (D) Cardiomyocyte cross-sectional area measurement in the border zone using the cell membrane marker WGA suggests that reduced cardiomyocyte cell size correlates with elevated *FGF10* levels (E; $r^2=0.6777$, $p=0.02$). (F) For all patients, the proportion of small ($<600\mu\text{m}^2$), medium ($600 < X < 800\mu\text{m}^2$) and large ($>800\mu\text{m}^2$) cardiomyocytes was determined. (G) Elevated *FGF10* levels correlate with low frequency of large cardiomyocyte ($>800\mu\text{m}^2$, $r^2=0.66$, $p=0.02$). (H-I) Histological Sirius red staining showed that elevated *FGF10* levels correlate with reduced fibrosis in the border zone ($r^2=0.7622$, $p=0.004$). Pictures, according to patient-corresponding *FGF10* levels depicted in (A), have been classified from low to high expression as represented by the above grey triangle. Scale bars 100 μm . Statistical significance (p) was determined using Student's t -distribution.